Journal of Quantitative Spectroscopy & Radiative Transfer 240 (2020) 106676

Contents lists available at ScienceDirect

Journal of Quantitative Spectroscopy & Radiative Transfer

journal homepage: www.elsevier.com/locate/jqsrt

Evaluation of different parameterizations of temperature dependences of the line-shape parameters based on *ab initio* calculations: Case study for the HITRAN database

N. Stolarczyk[a,*], F. Thibault[b], H. Cybulski[c], H. Jóźwiak[a], G. Kowzan[a], B. Vispoel[d], I.E. Gordon[e], L.S. Rothman[e], R.R. Gamache[d], P. Wcisło[a]

[a] Institute of Physics, Faculty of Physics, Astronomy and Informatics, Nicolaus Copernicus University in Torun, Grudziadzka 5, Torun 87–100, Poland
[b] Univ Rennes, CNRS, IPR (Institut de Physique de Rennes)-UMR 6251, F-35000 Rennes, France
[c] Institute of Physics, Kazimierz Wielki University, Plac Weyssenhoffa 11, Bydgoszcz 85-072, Poland
[d] Department of Environmental, Earth, and Atmospheric Sciences, University of Massachusetts Lowell, Lowell, MA, USA
[e] Harvard-Smithsonian Center for Astrophysics, Atomic and Molecular Physics Division, Cambridge, MA, USA

ARTICLE INFO

Article history:
Received 22 July 2019
Revised 23 September 2019
Accepted 25 September 2019
Available online 26 September 2019

Keywords:
Temperature dependence of spectroscopic line-shape parameters
Pressure broadening and shift
HITRAN Database
Molecular collisions
Spectral line shapes

ABSTRACT

Temperature dependences of molecular line-shape parameters are important for the spectroscopic studies of the atmospheres of the Earth and other planets. A number of analytical functions have been proposed as candidates that may approximate the actual temperature dependences of the line-shape parameters. In this article, we use our *ab initio* collisional line-shape calculations for several molecular systems to compare the four temperature ranges (4TR) representation, adopted in the HITRAN database [J. Quant. Spectrosc. Radiat. Transfer 2017;203:3] in 2016, with the double-power-law (DPL) representation. Besides the collisional broadening and shift parameters, we consider also the most important line-shape parameters beyond Voigt, i.e., the speed dependence of broadening and shift parameters, and real and imaginary parts of the complex Dicke parameter. We demonstrate that DPL gives better overall approximation of the temperature dependencies than 4TR. It should be emphasized that DPL requires fewer parameters and its structure is much simpler and more self-consistent than the structure of 4TR. We recommend the usage of DPL representation in HITRAN, and present DPL parametrization for Voigt and beyond-Voigt line profiles that will be adopted in the HITRAN database. We also discuss the problem of the Hartmann-Tran profile parametrization in which the correlation parameter, η, and frequency of the velocity-changing collisions parameter, ν_{vc}, diverges to infinity when collisional shift crosses zero; we recommend a simple solution for this problem.

1. Introduction

Knowledge of accurate molecular spectroscopic parameters is essential for interpreting and modeling spectra of terrestrial and planetary atmospheres, including those of exoplanets or even those of brown dwarfs. These parameters are provided in the HITRAN [1] and HITEMP [2] molecular spectroscopic databases. Broadening and shift of spectral lines due to the collisions of target molecules with those of ambient gases are among important parameters that need to be used in the opacity calculations. Traditionally, the HITRAN database provided the single temperature exponent to the power law, in order to extrapolate the value of the collisional half-width at half maximum from the reference value given at 296 K to any other temperature. This approach works fairly well within the temperature ranges encountered in the terrestrial atmosphere. Nevertheless, it is now well known that the power law with a single exponent does not work over a broader range of temperatures (see for instance [3–8]). Therefore, if one aims to model such parameters at very diverse temperatures that are encountered in different planetary atmospheres (for instance an average temperature on Uranus is about 55 K whereas those encountered on hot Jupiters [9] or lava planets [10] can reach 1000 - 2500 K), more sophisticated models have to be employed. Combustion applications also require more flexible solutions [5,7].

* Corresponding author.
E-mail addresses: NikodemStolarczyk319@gmail.com (N. Stolarczyk), Robert_Gamache@uml.edu (R.R. Gamache), piotr.wcislo@fizyka.umk.pl (P. Wcisło).

https://doi.org/10.1016/j.jqsrt.2019.106676

A number of approximations have been proposed as candidates that may represent the actual temperature dependences of the broadening, γ_0, and shift, δ_0, parameters, see the thorough discussion in the Introduction in Ref. [4]. One way of improving the single power-law approach for pressure broadening was to split it into four temperature ranges (4TR representation) [3]; in the case of the shift parameter, a linear function was split into the four ranges [3]. The 4TR approach was adopted in the 2016 edition of the HITRAN database [1].

Following previous works [11–14], a double-power-law (DPL) was recently proposed to approximate the temperature dependences of both the broadening and shift [4], see also Ref [15] for the review of the modern line-shape theory. It was shown that the DPL reproduces the temperature dependences much better than the single power-law function for broadening and linear function for shift [4].

In this paper, we directly compare the 4TR and DPL approaches for several molecular systems. For this purpose, we use our *ab initio* quantum scattering and semiclassical line-shape calculations. We observe that for the case of γ_0 the two methods work equally well, while for δ_0 the DPL approximation is better. It has to be emphasized, however, that for these two line-shape parameters (γ_0 and δ_0) DPL requires two times fewer parameters than 4TR.

Besides the two basic line-shape parameters (γ_0 and δ_0), we also performed the comparison between the 4TR and DPL approaches for the most important beyond-Voigt line-shape parameters describing the speed dependence of pressure broadening and shift (γ_2 and δ_2) and the velocity-changing collisions ($\widetilde{\nu}^{\mathrm{r}}_{\mathrm{opt}}$, and $\widetilde{\nu}^{\mathrm{i}}_{\mathrm{opt}}$). Concerning γ_2 and δ_2 parameters, the 4TR approach adopted in HITRAN2016 [1,3] assumed constant values of these parameters in each of the temperature ranges. In this case, the DPL approach gives a much better approximation despite that it requires the same number of parameters as 4TR. With respect to the $\widetilde{\nu}^{\mathrm{r}}_{\mathrm{opt}}$ and $\widetilde{\nu}^{\mathrm{i}}_{\mathrm{opt}}$ parameters, the approach adopted in HITRAN2016 [1,3] assumed a simple single power-law function; hence, the DPL approach introduced here obviously gives a much better approximation. In this paper, we also argue that, from the perspective of temperature dependence representation, it is better to use the direct approach ($\widetilde{\nu}^{\mathrm{r}}_{\mathrm{opt}}$ and $\widetilde{\nu}^{\mathrm{i}}_{\mathrm{opt}}$) instead of the $\widetilde{\nu}_{\mathrm{vc}}$ and η parametrization introduced in the Hartmann-Tran profile [16] (η and $\widetilde{\nu}_{\mathrm{vc}}$ diverge to infinity when the collisional shift crosses zero).

We show that DPL gives a better overall approximation of the temperature dependencies of the six line-shape parameters than 4TR, emphasizing that DPL requires fewer parameters and its structure is much simpler and more self-consistent than the structure of 4TR. We recommend the usage of DPL representation in HITRAN, and present DPL parametrization for Voigt and beyond-Voigt line profiles that will be adopted in the HITRAN database.

In Sections 2 and 3, we discuss the methodology and details of the fully quantum and semiclassical calculations, respectively. In Sections 4–6, we show the comparison of the two approaches for the (γ_0 and δ_0), (γ_2 and δ_2) and ($\widetilde{\nu}^{\mathrm{r}}_{\mathrm{opt}}$ and $\widetilde{\nu}^{\mathrm{i}}_{\mathrm{opt}}$) parameters. In Section 7, we demonstrate the definition of the names of the DPL parameter that will be adopted in HITRAN.

2. *Ab initio* quantum line-shape calculations

In this section, we briefly describe the calculations based on the close-coupling scheme and we give some details of the potential energy surfaces (PESs) for systems considered here. In the case of diatomic molecules, an interaction energy, in general, depends on the angular orientation of the collisional partners, distance between their centers of mass (the intermolecular distances), and, if applicable, intramolecular distances. For the purpose of solving the close-coupling equations, the dependence on the intermolecular distance is extracted from a multidimensional PES. This is done in two steps. First, the PES is expanded in the complete basis of orthonormal angular functions, either bispherical harmonics (see, for example Eq. (4) in Ref. [17] and Appendix therein) or Legendre polynomials (see Eq. (1) in Ref. [18]), if two colliding diatomic molecules or a diatomic molecule colliding with an atom are concerned, respectively. The coefficients of such an expansion depend only on the intra- and intermolecular distances. Second, the intramolecular dependence of the interaction energy is reduced by projecting the obtained coefficients on the wavefunctions of the colliding partners (see Eq. (2) in Ref. [18] and the discussion therein). The number of resulting radial terms, employed in the further calculations, depends on the investigated system (see Sections 2.1–2.4). These terms are used during solving the close-coupling equations [19]. Boundary conditions on the wavefunctions of a scattering system relate the solutions of the close-coupling equations with the elements of the scattering matrix (S-matrix). The S-matrix itself is used in the calculations of the generalized spectroscopic cross sections, $\sigma^q_\lambda(v_i, j_i, v_f, j_f, j_2; E_{\mathrm{kin}})$ [20–24]. Here, v_i, v_f, and j_i, j_f are, respectively, the initial and final vibrational and rotational quantum numbers of the optically active molecule. j_2 is the rotational quantum number of the perturbing molecule (being equal to 0 when the perturber is an atom), λ is the rank of the velocity tensor, q is the tensorial rank of the radiation-matter interaction, and E_{kin} is the relative kinetic energy of the colliding pair. The speed-averaged pressure broadening, γ_0, and shift, δ_0, parameters can be obtained from purely *ab initio* calculations. They are connected with the generalized spectroscopic cross sections by the following formula:

$$\begin{aligned}\Gamma_0(T) + i\Delta_0(T) &= (\gamma_0(T) + i\delta_0(T))p \\ &= \frac{1}{2\pi c} n\langle v_r\rangle \sum_{j_2} p_{j_2}(T) \\ &\quad \times \int \mathrm{d}x\, x e^{-x} \sigma_0^q\left(v_i, j_i, v_f, j_f, j_2; E_{\mathrm{kin}} = x k_{\mathrm{B}} T\right), \quad (1)\end{aligned}$$

where n is the number density of perturbing molecules, c is the speed of light in vacuum, T is the temperature, $\langle v_r\rangle$ is the mean relative speed of the colliding partners and p_{j_2} is the population of the j_2-th state of the perturber molecule at the temperature T.

The γ_0 and δ_0 parameters are the speed-averaged values of pressure broadening and shift parameters. Even though the exact, active molecule, speed dependence, $\gamma(v)$ and $\delta(v)$, can be determined numerically with the *ab initio* calculations, it is difficult to represent them in the spectroscopic databases. To address this problem, the speed dependence is expressed in terms of the quadratic approximation [25–27]:

$$\gamma(v) + i\delta(v) \approx \gamma_0 + i\delta_0 + (\gamma_2 + i\delta_2)\left(\frac{v^2}{v_m^2} - \frac{3}{2}\right), \quad (2)$$

with v_m being the most probable (absolute) speed. The parameters γ_2 and δ_2 can be expressed as a function of temperature [28]:

$$\gamma_2(T) + i\delta_2(T) = \frac{v_m}{2}\frac{d}{dv}\sum_{j_2} p_{j_2}(T)\Big(\gamma(v) + i\delta(v)\Big)\Big|_{v=v_m}. \quad (3)$$

We provide the exact formulas for $\gamma(v)$ and $\delta(v)$ in Appendix C.

Similarly to γ_0 and δ_0, the Dicke parameter, $\widetilde{\nu}_{\mathrm{opt}}$, can also be obtained from purely *ab initio* calculations, based on the generalized spectroscopic cross sections [28,29]:

$$\begin{aligned}\nu_{\mathrm{opt}}(T) = \widetilde{\nu}_{\mathrm{opt}}(T)p &= \frac{1}{2\pi c} n\langle v_r\rangle M_2 \sum_{j_2} p_{j_2}(T) \\ &\quad \times \int_0^\infty dx\, x e^{-x}\Big(\frac{2}{3} x \sigma_1^q\left(v_i, j_i, v_f, j_f, j_2; E_{\mathrm{kin}} = x k_{\mathrm{B}} T\right) \\ &\quad - \sigma_0^q\left(v_i, j_i, v_f, j_f, j_2; E_{\mathrm{kin}} = x k_{\mathrm{B}} T\right)\Big), \quad (4)\end{aligned}$$

where $M_2 = \frac{m_p}{m+m_p}$, with m and m_p being the masses of the active and perturbing molecules, respectively.

Eqs. (1), (3) and (4) are general expressions illustrating how to calculate the temperature dependence of the spectroscopic parameters from first principles. In Sections 4–6 we discuss how well they can be approximated with the DPL and 4TR representations.

It should be noted that the fully *ab initio* line-shape parameters are best suited with the sophisticated line-shape models that include the full *ab initio* speed dependence and reliable model of the velocity-changing collisions (such as billiard-ball [30,31] or Blackmore [32] profiles). If the *ab initio* line-shape parameters are directly used with simple phenomenological profiles based on hard- or soft-collision models and approximated forms of the speed dependencies of the pressure broadening and shift (such as the Hartmann-Tran profile [16,33,34]), one should expect additional percent-level discrepancy with experimental line profiles (for some atypical systems, such as Ar-perturbed H_2, this discrepancy is much larger). Depending on the molecular system, different strategies may be applied to reduce these errors. For instance, for systems exhibiting large Dicke narrowing a correcting function (called beta-correction) to the $\widetilde{\nu}_{\text{opt}}$ parameter can be used to improve the performance of the hard-collision model [35]. Recently, Hartmann proposed a general approach to this problem [36], in which the *ab initio* line-shape parameters are used with one of the sophisticated line-shape models to generate reference shapes in a wide range of pressures, and then the reference spectra are fitted with some simpler phenomenological model. In this scheme the fitted line-shape parameters lose their physical meaning, but the shapes of molecular lines better agree with experiment. Similar tests were done before, for instance see Ref. [37] (in that work, due to a lack of *ab initio* parameters, a sophisticated line-shape model was used with parameters determined experimentally). Recently, this approach was tested for the requantized Classical Molecular Dynamics Simulations corrected with the use of experimental spectra [38].

2.1. H_2-He

Here, we employ the recently reported, three-dimensional (3D) PES [29], which is an extension of the PES reported in Ref. [39]. The PES from Ref. [39] was argued [18] to be the most reliable among all the considered PESs in terms of reproducing the experimental data. The newer PES [29] covers a larger range of intramolecular distances than the previous one, which allows us to investigate the overtones. Moreover, this PES has better long range asymptotic behavior.

The PES was expanded over Legendre polynomials, and then averaged over the wavefunctions of the hydrogen molecule in the initial and final rovibrational states. This led to 2×4 radial terms per each rovibrational transition and 144 terms for purely rotational transitions (for details see Section 3.3 of Ref. [29] and Section 2 of Ref. [40]).

The close-coupling equations were solved for about 260 values of kinetic energy in a range from 0.1 up to 9000 cm^{-1}. In the calculations we used the log-derivative/Airy hybrid propagator [41]. The log-derivative method was used for the intermolecular distances in a range from 1 to 20 a_0 and the Airy propagator for intermolecular distances in a range from 20 to 100 a_0. Due to the fact that the PES does not couple *ortho* and *para* states, we dealt with separate basis sets for these two cases, associated with odd or even values of rotational levels j. One asymptotic closed level was kept throughout all the calculations.

For the present study we investigated the following lines: O(2) 0-0, O(3) 2-0, Q(1) 2-0, Q(1) 4-0, Q(3) 5-0, S(0) 0-0, S(0) 1-0, S(1) 1-0, and S(1) 9-0.

2.2. H_2-H_2

For the H_2-H_2 system we used the 6D PES reported in Ref. [42]. This PES is a combination of two previous PESs: the 6D PES of Hinde [43], which takes into account the stretching of both hydrogen molecules, and the 4D PES of Patkowski *et al.* [44], calculated with rigid hydrogen monomers with the bond length set to the vibrational ground-state averaged value. The PES from Ref. [42] was expanded over the bispherical harmonics, leading to 15 terms, which were later averaged over the wavefunctions of the hydrogen molecule.

The close-coupling equations were solved for about 250 values of kinetic energy between 0.1 and 5000 cm^{-1}. We used the log-derivative/Airy hybrid propagator [41] with the log-derivative method active in the range from 2.5 to 30 a_0 and Airy propagator between 30 and 50 a_0. The calculations were performed for the rotational levels of the perturbing molecule, j_2, from 0 up to 5. Similar to the H_2-He system, we analyzed the transitions between the *ortho* and *para* states separately. We investigated the electric quadrupole ($q = 2$) $Q_v(1)$ lines of the fundamental band and of the first overtone.

2.3. CO-He

The $^{12}C^{16}O$ rovibrational energy levels, used in the basis for the CO-He and CO-Ar dynamical calculations, are those provided by the HITRAN2016 database. The energy levels of CO in HITRAN2016 are based on Li *et al.* [45] with some corrections associated with the implementation of the Coxon and Hajigeorgiou potential [46]. The dynamical calculations were performed on the 3D CO-He PES of Heijmen *et al.* [47]. A Fortran code provided by van der Avoird [47] contains the vibrationally averaged PES in the fundamental and first excited vibrational states of $^{12}C^{16}O$. The resulting PESs have been expanded over 14 Legendre polynomials (up to l=13). The close-coupling calculations are very similar to the ones performed on these PESs, in Ref. [48] and, thus, will not be described. In order to deduce the pressure broadening and shift coefficients for the purely rotational and rovibrational R(0) 0-0, R(0) 1-0, R(20) 0-0 and R(20) 1-0 lines, necessary [48] S-matrix elements were computed for about 180 and 140 relative kinetic energies, ranging from 0.1 to 2000 cm^{-1}, for the R(0) 0-0, R(0) 1-0, R(20) 0-0 and R(20) 1-0 lines, respectively.

2.4. CO-Ar

The PES used for the calculations of CO-Ar cross sections was the purely *ab initio* potential calculated by Sumiyoshi and Endo [49]. The C-O bond length values, r_{CO}, spanned a range from 1.00 Å to 1.35 Å in increments of 0.05 Å. This range of r_{CO} covers 99.98% of the squared wavefunction amplitude of the upper vibrational state ($v = 1, j = 0$), what we consider sufficient for calculations of $v = 0 \rightarrow 1$ transitions. The PES was vibrationally averaged over the lower and upper vibrational states and expanded in the basis of Legendre polynomials with terms up to the $n = 10$ order.

The S-matrices were calculated with the log-derivative/Airy hybrid propagator [41]. The log-derivative method was used from 2 Å to 10 Å and the Airy propagator was used from 10 Å to the end of propagation. The end of propagation was set no closer than the CO-Ar distance of 20 Å. It was increased to the separation at the furthest classical turning point found in the centrifugal potential if the point was found to be lying further than 20 Å. The grid of collision energies at which the S-matrices were obtained consisted of 376 points. It was limited by the maximal energy of 1700 cm^{-1} and the grid density was adjusted to obtain smooth σ_0^q curves, with denser sampling at low collision energies and sparser sampling at high collision energies. The lines of the fundamental band

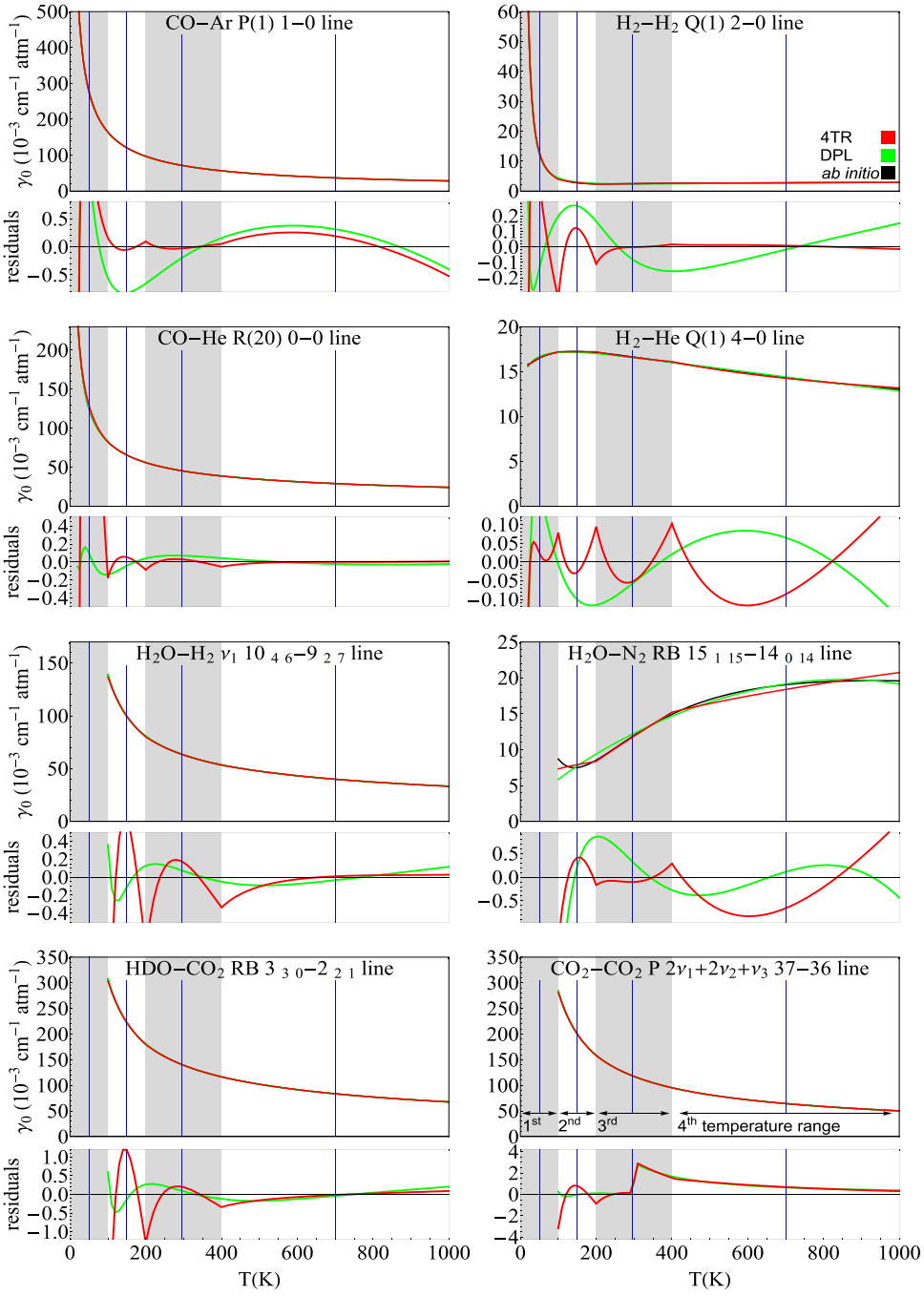

Fig. 1. *Ab initio* temperature dependences of the pressure broadening parameter γ_0, (black lines) and its 4TR and DPL approximations (red and green lines, respectively). To resolve overlapped curves below every graph we show the absolute residuals (the same color notation). The first temperature range is not covered by the semiclassical MCRB calculations. The residuals are in the same units as the main plots, i.e., 10^{-3}cm^{-1}atm^{-1}.

for which the spectroscopic cross sections were obtained are: P(1), P(2), P(8), R(0), R(1), and R(7).

3. *Ab initio* semiclassical line-shape calculations

The calculation of the half-width and line shift for the H_2O-H_2, H_2O-N_2, HDO-CO_2 and CO_2-CO_2 systems were made using the complex implementation of the semi-classical Robert-Bonamy formalism [50,51] with the modification suggested by Ma [52], labeled as MCRB. In this complex-valued formalism, the half-width, γ, and line shift, δ, for a rovibrational transition f ← i are given by

$$\begin{aligned}\Gamma_0(T) + i\Delta_0(T) &= (\gamma_0(T) + i\delta_0(T))p \\ &= \frac{1}{2\pi c} n \int_0^\infty \mathrm{d}v_r\, v_r f(v_r) \\ &\quad \times \int_0^\infty \mathrm{d}b\, 2\pi b \left(1 - e^{-i\langle S_1 + Im(S_2)\rangle_{J_2}} e^{-\langle Re(S_2)\rangle_{J_2}}\right), \quad (5)\end{aligned}$$

where v_r is the relative velocity, $f(v_r)$ is the Maxwell-Boltzmann distribution of speed, $\langle\rangle_{J_2}$ is an average over the states of the perturber, and b is the impact parameter. S_1 and S_2 are the first and second order terms in the successive expansion of the Liouville

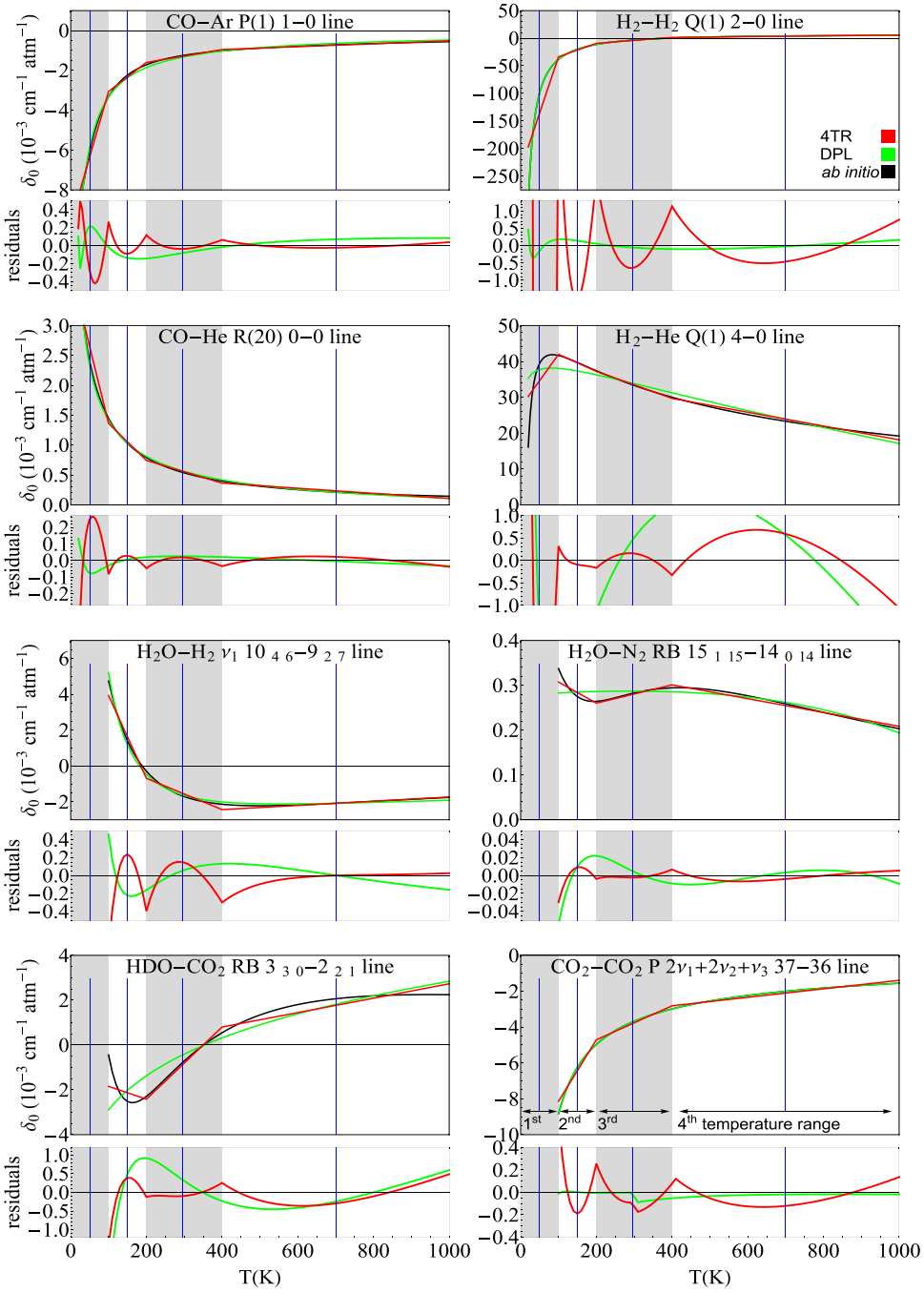

Fig. 2. *Ab initio* temperature dependences of the pressure shift parameter δ_0, (black lines) and its 4TR and DPL approximations (red and green lines, respectively). To resolve overlapped curves below every graph we show the absolute residuals (the same color notation). The first temperature range is not covered by the semiclassical MCRB calculations. The residuals are in the same units as the main plots, i.e., $10^{-3}\mathrm{cm}^{-1}\mathrm{atm}^{-1}$.

scattering matrix, which depends on the rovibrational states that are involved, the associated collisionally-induced jumps from these states, on the intermolecular potential, and the characteristics of the collision dynamics. Note, semiclassical refers to the fact that the internal structure of the colliding molecules is treated quantum mechanically and that the dynamics of the collision process are treated by classical mechanics. Thus, in an optical transition from f ← i, the active molecule will undergo collisions with the bath molecules, for which the trajectories are determined by classical mechanics. In these collisions, the initial and final states of the radiating molecule, i and f, will undergo collisionally-induced transitions to states i' and f', interrupting the radiation and causing collisional broadening. The states i' and f' are called collisionally-connected states and are given by selection rules determined by the wavefunctions and intermolecular potential coupling terms. Given the large number of terms in the intermolecular potential, there are many states, i' or f', that are possible. The quantum mechanical components of the calculation are the energy of the states involved in the collisionally-induced transitions and the wavefunctions for the states, which are used to determine the probability of

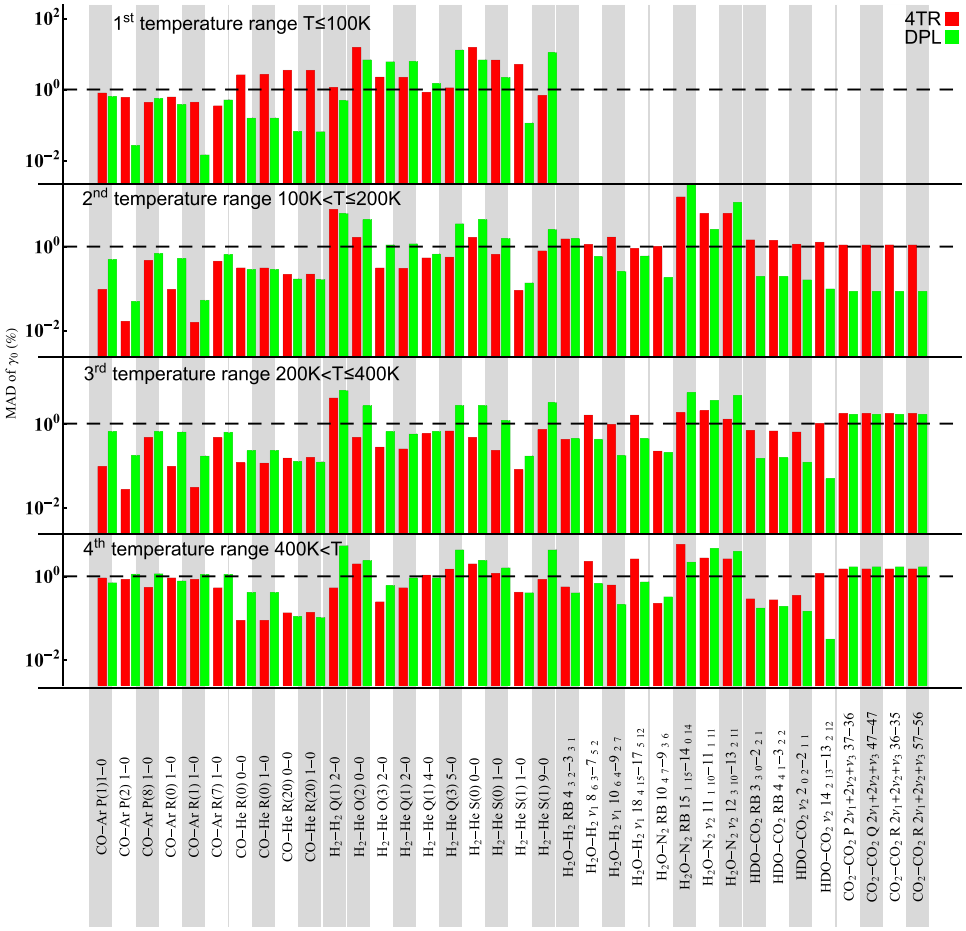

Fig. 3. The relative MAD for the 4TR and DPL representations of the temperature dependence of the pressure broadening parameter γ_0 (see text for more details). The 1% level is indicated with the horizontal black dashed lines. The first temperature range is not covered by the semiclassical MCRB calculations.

a collisionally-induced transition. The details about our calculations for the H_2O-H_2, H_2O-N_2, HDO-CO_2 and CO_2-CO_2 systems considerd here can be found in Refs. [53–56].

4. Temperature dependences of the pressure broadening and shift parameters γ_0 and δ_0

In this section, we directly compare the two representations (4TR and DPL) of the temperature dependences of the pressure broadening, γ_0, and pressure shift, δ_0, parameters. In Section 4.1, we discuss the details of the 4TR [1,3] and DPL [4] approaches. The 4TR approach requires eight parameters (two parameters per each temperature range) to describe the full temperature dependence of a single line-shape parameter, while the DPL requires only four parameters (in the DPL case a single function covers all the temperature ranges). In Section 4.2, we present the results and the comparison of the two representations.

4.1. 4TR and DPL representations of γ_0 and δ_0

The 4TR representation (in the form adopted in HITRAN2016 [1,3]) splits the temperature dependence into four ranges, each represented by a different reference temperature, T_{ref}:

1st range: $T < 100$ K, $T_{ref} = 50$ K,
2nd range: 100 K $\leq T <$ 200 K, $T_{ref} = 150$ K,
3rd range: 200 K $\leq T <$ 400 K, $T_{ref} = 296$ K,
4th range: 400 K $\leq T$, $T_{ref} = 700$ K.

In each of the four ranges, the temperature dependences of γ_0 and δ_0 are described by the power-law and linear functions:

$$\gamma_0(T) = \gamma_0(T_{ref}) \times \left(\frac{T_{ref}}{T}\right)^n, \quad (6)$$

$$\delta_0(T) = \delta_0(T_{ref}) + \delta_0'(T - T_{ref}). \quad (7)$$

This representation requires a pair of fitted parameters, $\gamma_0(T_{ref})$ and n, or $\delta_0(T_{ref})$ and δ_0', for each of the four ranges, resulting in eight parameters in total for each of the two (γ_0 and δ_0) spectral line-shape parameters. Additionally, we enforced the functions to be continuous between the ranges, which resulted in three additional constraints. To fit these representations to the *ab initio* data, we performed a two-step fitting procedure using the least-squares method. In the first step, we used the fitting algorithm for the 2nd and 3rd temperature ranges (most important for the studies of atmospheres of the Earth and other planets), demanding the continuity at T = 200 K. In the next step, we performed the fitting for the remaining 1st and 4th temperature ranges, demanding the fitted functions (Eqs. (6) and (7)) to be continuous on the two other borders, i.e. at T = 100 K and T = 400 K.

Recently, Gamache and Vispoel proposed the DPL representation for γ_0 and δ_0 [4] (here the names of the parameters are changed to be consistent with naming for other line-shape parameters):

$$\gamma_0(T) = g_0(T_{ref}/T)^n + g_0'(T_{ref}/T)^{n'}, \quad (8)$$

$$\delta_0(T) = d_0(T_{ref}/T)^m + d_0'(T_{ref}/T)^{m'}. \quad (9)$$

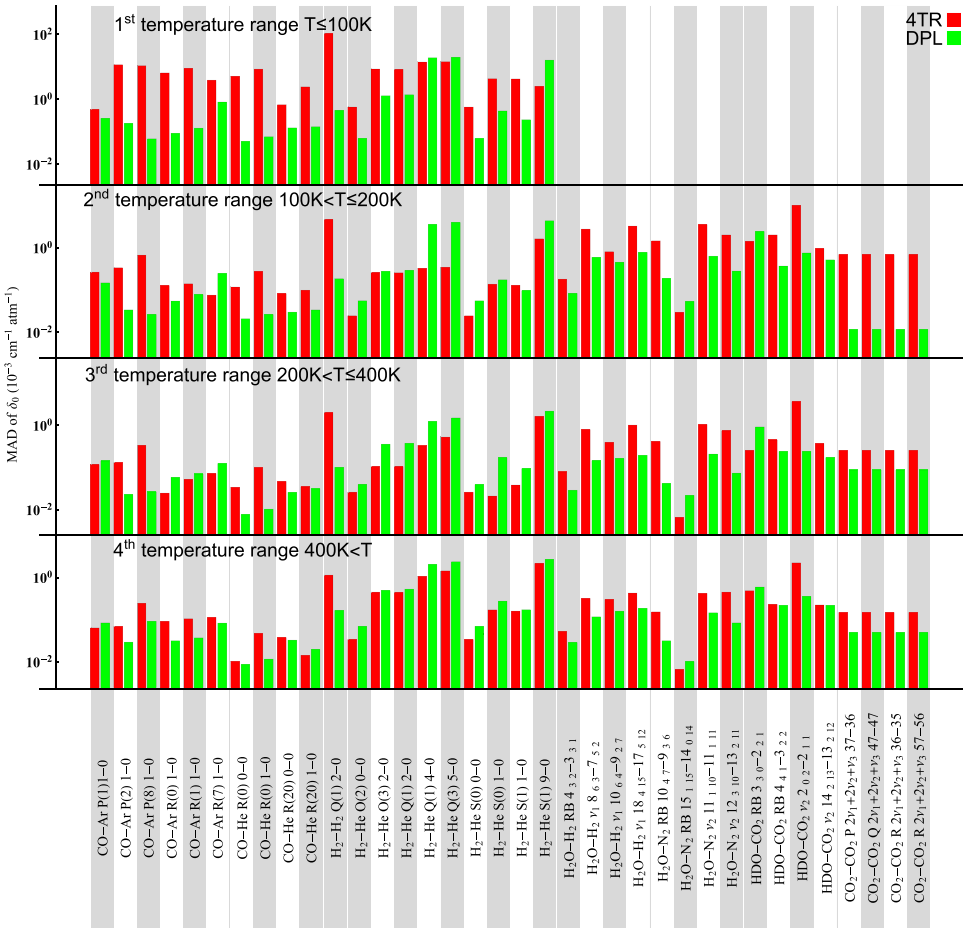

Fig. 4. The MAD for the 4TR and DPL representations of the temperature dependence of the pressure shift parameter, δ_0 (see text for more details). The first temperature range is not covered by the semiclassical MCRB calculations.

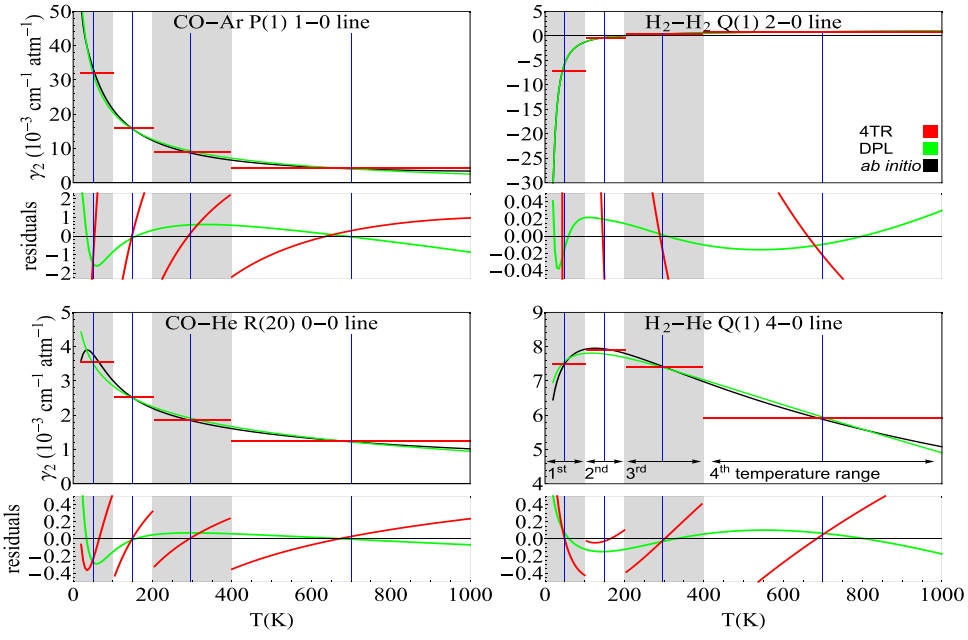

Fig. 5. Temperature dependence of the speed dependence of the broadening parameter, γ_2. The black lines are the functions determined from our *ab initio* calculations, while red and green ones are the 4TR and DPL representations, respectively. To resolve overlapped curves below every graph we show the absolute residuals (the same color notation). The residuals are in the same units as the main plots, i.e., 10^{-3}cm^{-1}atm^{-1}.

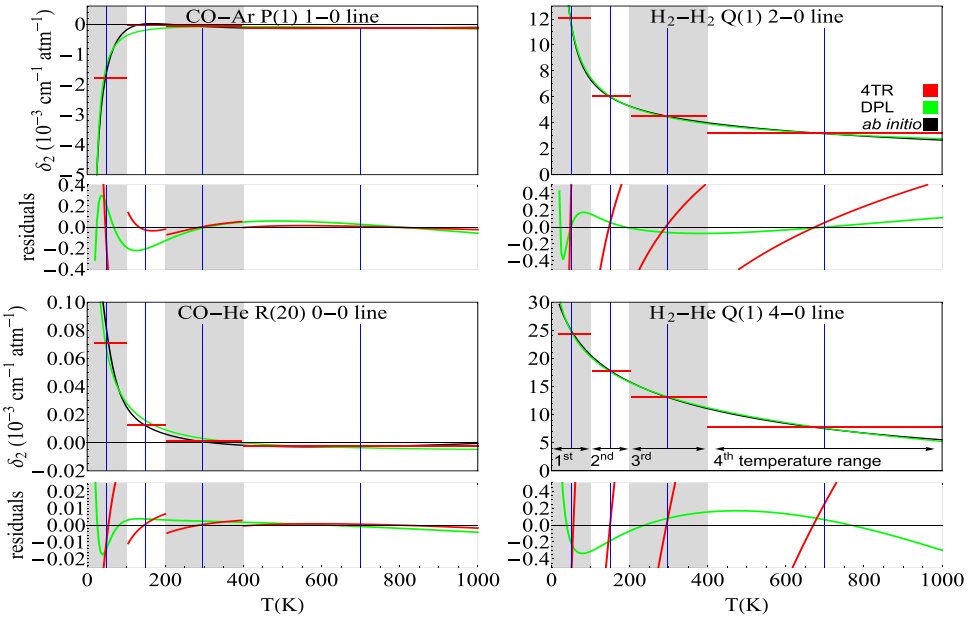

Fig. 6. Temperature dependence of the speed dependence of the shift parameter, δ_2. The black lines are the functions determined from our *ab initio* calculations, while red and green ones are the 4TR and DPL representations, respectively. To resolve overlapped curves below every graph we show the absolute residuals (the same color notation). The residuals are in the same units as the main plots, i.e., 10^{-3}cm^{-1}atm^{-1}.

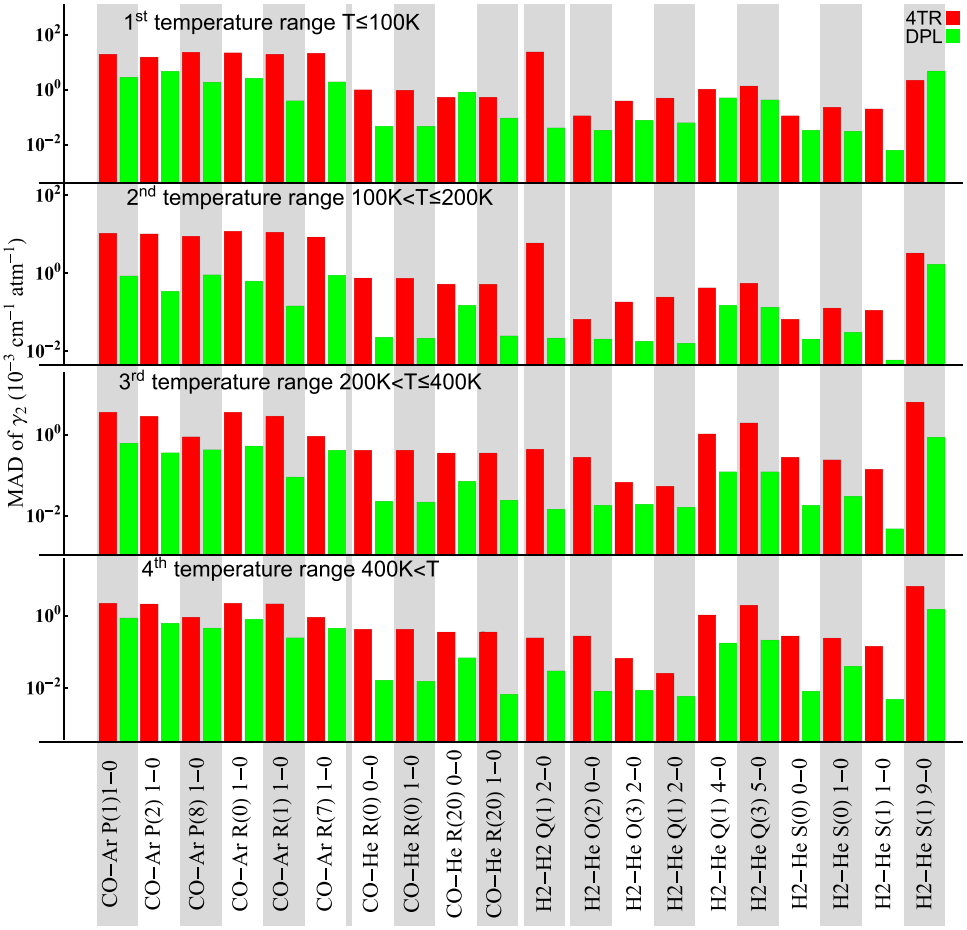

Fig. 7. The MAD for the 4TR and DPL representations of the temperature dependence of the speed dependence of the broadening parameter, γ_2 (see text for more details).

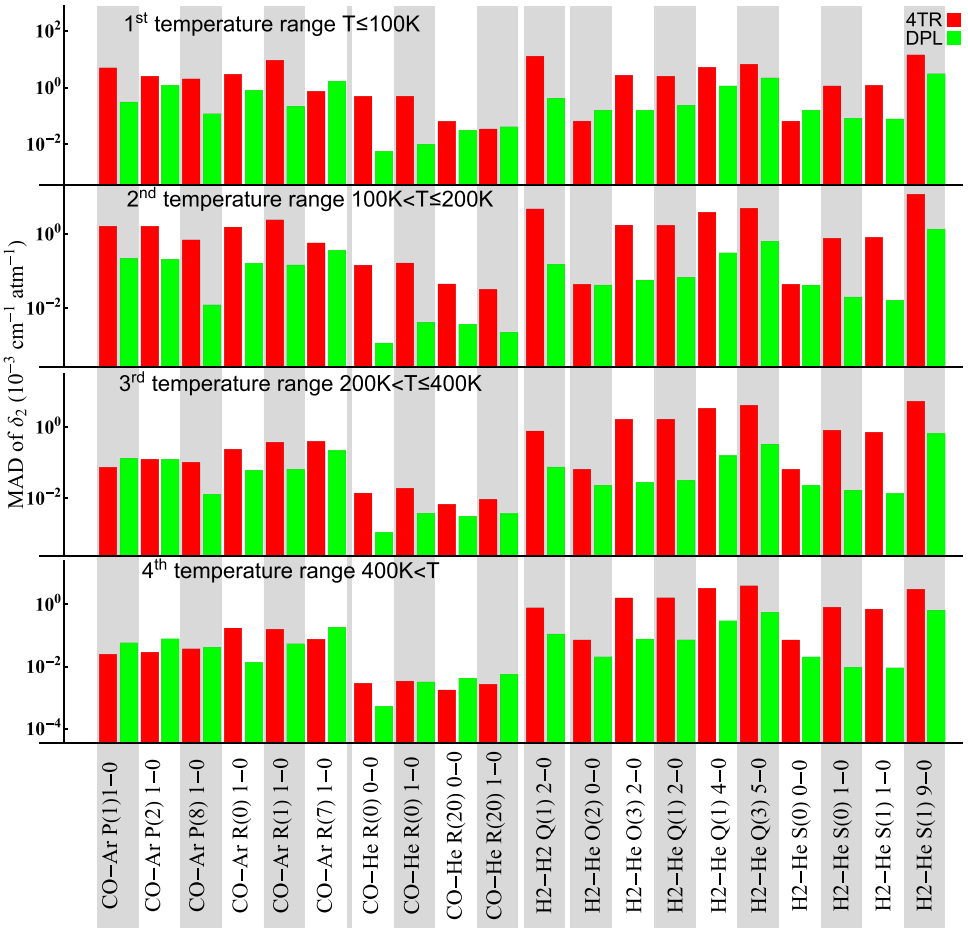

Fig. 8. The MAD for the 4TR and DPL representations of the temperature dependence of the speed dependence of the shift parameter, δ_2 (see text for more details).

A single DPL function covers all the temperature ranges. The reference temperature, T_{ref}, is 296 K. This representation requires four parameters (two times fewer than 4TR) to represent the full temperature dependence of the spectral line-shape parameter and has no additional constraints. We used the least squares algorithm to fit this representation to the *ab initio* data.

4.2. Results and comparison

The two representations (4TR and DPL) were tested on the *ab initio* results for a sample of 36 molecular lines from eight collisional systems. We employed the fully quantum *ab initio* calculations for the CO-Ar, CO-He, H_2-He and H_2-H_2 systems, while the calculations for the H_2O-H_2, H_2O-N_2, HDO-CO_2 systems were based on the *ab initio* semiclassical approach. The full temperature dependences of the eight chosen rovibrational transitions (one for each molecular system) are shown in Figs. 1 and 2 for the cases of γ_0 and δ_0, respectively. Figs. 3 and 4 present the comparison of the maximal absolute difference (MAD) for both approximations for all the considered lines.

It is seen from Figs. 1 and 3 that (despite that DPL requires two times fewer parameters) both approximations give similar accuracy of γ_0 representation, and in the prioritized 2nd and 3rd temperature ranges MAD is at the level of 1% in most of the cases.

Figs. 2 and 4 show the comparison of 4TR and DPL for the δ_0 parameter. For the typical (monotonic) behavior of the temperature dependences of δ_0, the DPL works better (CO-He, H_2O-N_2, CO_2-CO_2 and H_2-H_2 cases in Fig. 2) or similarly (CO-Ar and HDO-CO_2 cases in Fig. 2) to 4TR; it should be noted that also here the 4TR requires twice as many parameters as DPL. If, however, the temperature dependence has a minimum or maximum (e.g., H_2-He case in Fig. 2), the 4TR reveals more flexibility due to the larger number of the fitted parameters and, hence, gives a better accuracy of temperature dependence representation.

5. Temperature dependences of the pressure broadening and shift speed dependence parameters, γ_2 and δ_2

In this section, we shall make a similar comparison as presented in Section 4. Here, we discuss the temperature dependence of the speed dependence of the pressure broadening and shift coefficients, γ_2 and δ_2. We limit the discussion to the 20 molecular lines for which we performed the fully quantum calculations. In Section 5.1, we discuss the details of 4TR approach in the form adopted in HITRAN2016 [1,3] and DPL representation [4]. Both the approximations require four parameters to describe the full temperature dependence of the γ_2 and δ_2 parameters. Section 5.2 contains the comparison of the two representations and discussion of the results.

5.1. 4TR and DPL representations of γ_2 and δ_2

For the case of the γ_2 and δ_2 parameters, the form of the 4TR approximation adopted in HITRAN2016 requires four parameters [1,3]; it was assumed that γ_2 and δ_2 are constant over each of the temperature ranges:

$$\gamma_2(T) = \gamma_2(T_{ref}), \tag{10}$$

$$\delta_2(T) = \delta_2(T_{ref}), \tag{11}$$

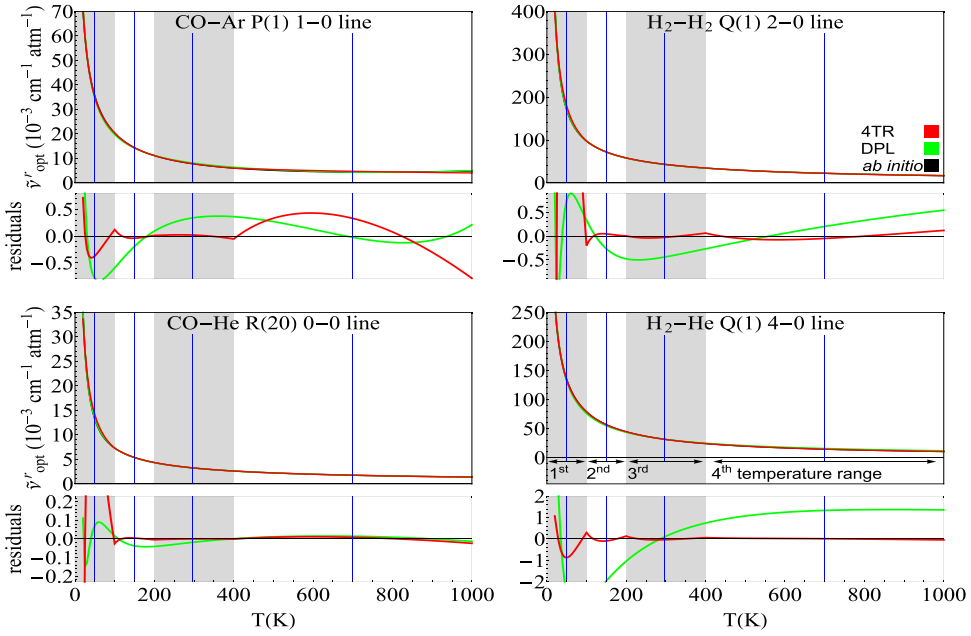

Fig. 9. *Ab initio* temperature dependences of the real part of the Dicke parameter, $\tilde{\nu}^{r}_{opt}$, (black lines) and its 4TR and DPL approximations (red and green lines, respectively). To resolve overlapped curves below every graph we show the absolute residuals (the same color notation). The residuals are in the same units as the main plots, i.e., $10^{-3}\mathrm{cm}^{-1}\mathrm{atm}^{-1}$.

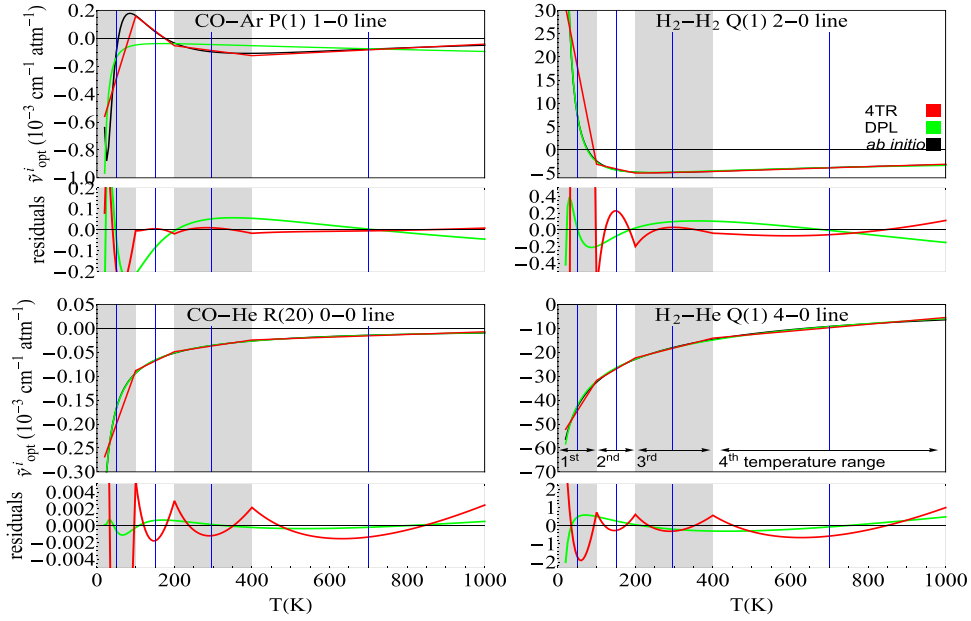

Fig. 10. *Ab initio* temperature dependences of the imaginary part of the Dicke parameter, $\tilde{\nu}^{i}_{opt}$, (black lines) and its 4TR and DPL approximations (red and green lines, respectively). To resolve overlapped curves below every graph we show the absolute residuals (the same color notation). The residuals are in the same units as the main plots, i.e., $10^{-3}\mathrm{cm}^{-1}\mathrm{atm}^{-1}$.

where T_{ref} takes one of the four values specified in Section 4.1. This representation requires one fitted parameter per each temperature range, resulting in four parameters in total.

The DPL approximations for the case of the γ_2 and δ_2 parameters have exactly the same form as for γ_0 and δ_0:

$$\gamma_2(T) = g_2(T_{ref}/T)^{j} + g_2'(T_{ref}/T)^{j'}, \quad (12)$$

$$\delta_2(T) = d_2(T_{ref}/T)^{k} + d_2'(T_{ref}/T)^{k'}. \quad (13)$$

with the same $T_{ref} = 296$ K.

5.2. Results and comparison

In the cases of the γ_2 and δ_2 parameters, we performed the same comparisons of the 4TR and DPL approaches as for γ_0 and δ_0 (see Section 4.2). The full temperature dependences of γ_2 and δ_2 for the same sample of the four molecular transitions as in Figs. 1 and 2 are presented in Figs. 5 and 6. Figs. 7 and 8 show the MAD for all the 20 analyzed transitions. The DPL method is better by far in almost all the considered cases, despite that it requires the same number of fitted parameters.

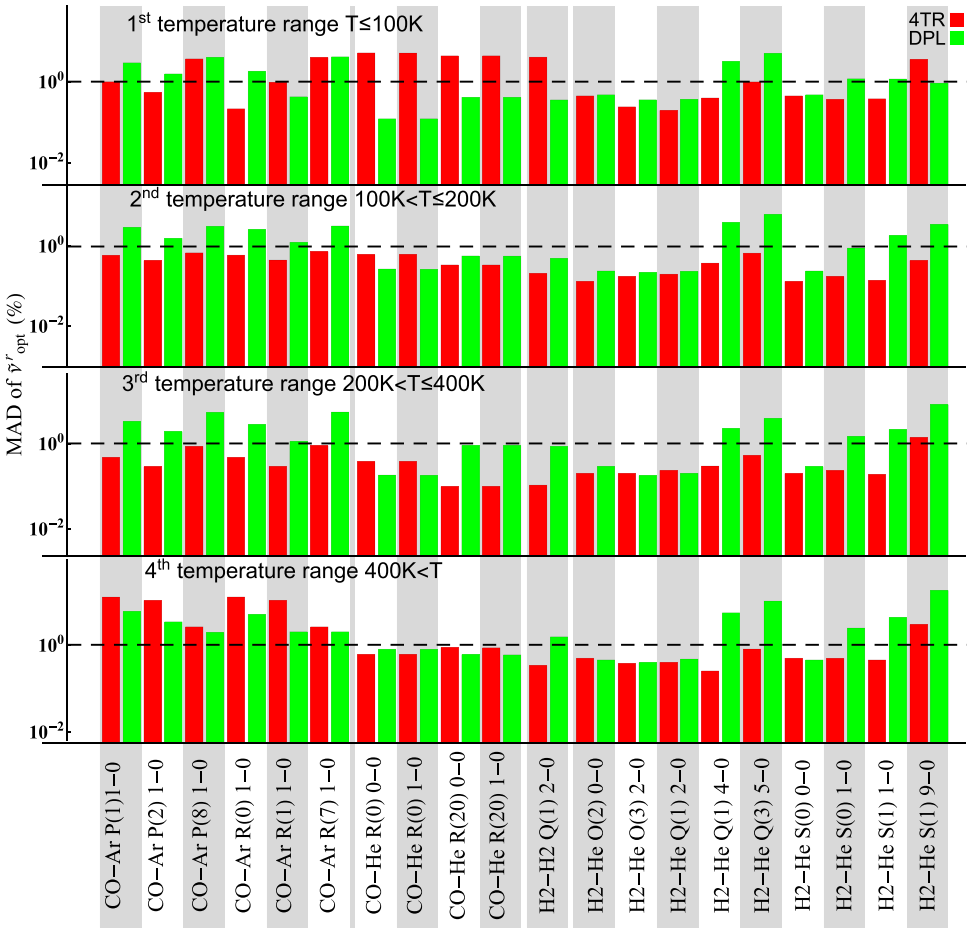

Fig. 11. The MAD for the 4TR and DPL representations of the temperature dependence of the real part of the Dicke parameter, $\tilde{\nu}^{r}_{opt}$ (see text for more details).

6. Temperature dependences of the Dicke parameter, $\tilde{\nu}_{opt}$

The four line-shape parameters discussed in Sections 4 and 5, in fact, can be seen as real and imaginary parts of two complex parameters. The first one, $\gamma_0 + i\delta_0$, is a complex rate of relaxation of optical excitation. The second one, $\gamma_2 + i\delta_2$, quantifies the speed dependence of this rate. Similarly, the rate of the optical velocity-changing collisions, $\tilde{\nu}_{opt}$, (also called the Dicke parameter) is also a complex number that can be written in the same manner, $\tilde{\nu}_{opt} = \tilde{\nu}^{r}_{opt} + i\tilde{\nu}^{i}_{opt}$, where $\tilde{\nu}^{r}_{opt}$ and $\tilde{\nu}^{i}_{opt}$ are called real and imaginary parts of the Dicke parameter, respectively.

It should be noted that in the Hartmann-Tran (HT) profile [16,33,34] the two parts of $\tilde{\nu}_{opt}$ are expressed indirectly with the use of $\tilde{\nu}_{vc}$ and η parameters:

$$\tilde{\nu}^{r}_{opt} = \tilde{\nu}_{vc} - \eta\gamma_0, \tag{14}$$

$$\tilde{\nu}^{i}_{opt} = -\eta\delta_0. \tag{15}$$

To calculate η and $\tilde{\nu}_{vc}$ we convert our *ab initio* $\tilde{\nu}_{opt}$ parameter (obtained from Eq. (4)) using the following formulas:

$$\tilde{\nu}_{vc} = \tilde{\nu}^{r}_{opt} - \tilde{\nu}^{i}_{opt}\frac{\gamma_0}{\delta_0}, \tag{16}$$

$$\eta = -\frac{\tilde{\nu}^{i}_{opt}}{\delta_0}. \tag{17}$$

It should be noted that the above relations, Eqs. (14)–(17), ignore the speed dependence of the $\tilde{\nu}_{opt}$ parameter which was adopted in the HT profile. We show in *Appendix B* that the HT profile enforces an unphysical form of the speed dependence of the complex Dicke parameter. Within the HT profile parametrization there is no flexibility to adjust the speed dependence of $\tilde{\nu}_{opt}$ to a more physical one. Therefore, the best that can be done to link the HT profile parameters with the *ab initio* ones is to enforce that the speed-averaged values of the complex Dicke parameter are the same; this is what we did in Eqs. (14)–(17).

The same parametrization as in the HT profile was adopted in HITRAN2016 [1,3] to represent the non-Voigt line profiles. In this paper, we argue that the more straightforward notation, i.e. $\tilde{\nu}_{opt} = \tilde{\nu}^{r}_{opt} + i\tilde{\nu}^{i}_{opt}$, allows one to avoid some additional difficulties with the temperature dependences that may arise when the $\tilde{\nu}_{vc}$ and η parametrization is used, see *Appendix A*. We recommend the use of the explicit notation of the real and imaginary parts of the Dicke parameter, i.e. $\tilde{\nu}_{opt} = \tilde{\nu}^{r}_{opt} + i\tilde{\nu}^{i}_{opt}$, and to neglect its speed dependence. For details of the DPL representation for the HITRAN database see Section 7.

6.1. 4TR and DPL representations of $\tilde{\nu}^{r}_{opt}$ and $\tilde{\nu}^{i}_{opt}$

Since the notation of the complex Dicke parameter recommended in this paper differs from the one adopted in HITRAN2016 [1,3] (i.e., we use $\tilde{\nu}^{r}_{opt}$ and $\tilde{\nu}^{i}_{opt}$ instead of $\tilde{\nu}_{vc}$ and η), here we do not compare the DPL and HITRAN2016 temperature dependences in a direct way (see *Appendix A* for a direct comparison). Nevertheless, to show the flexibility of the DPL approximation for the case of the Dicke parameter, we compare it with the 4TR rep-

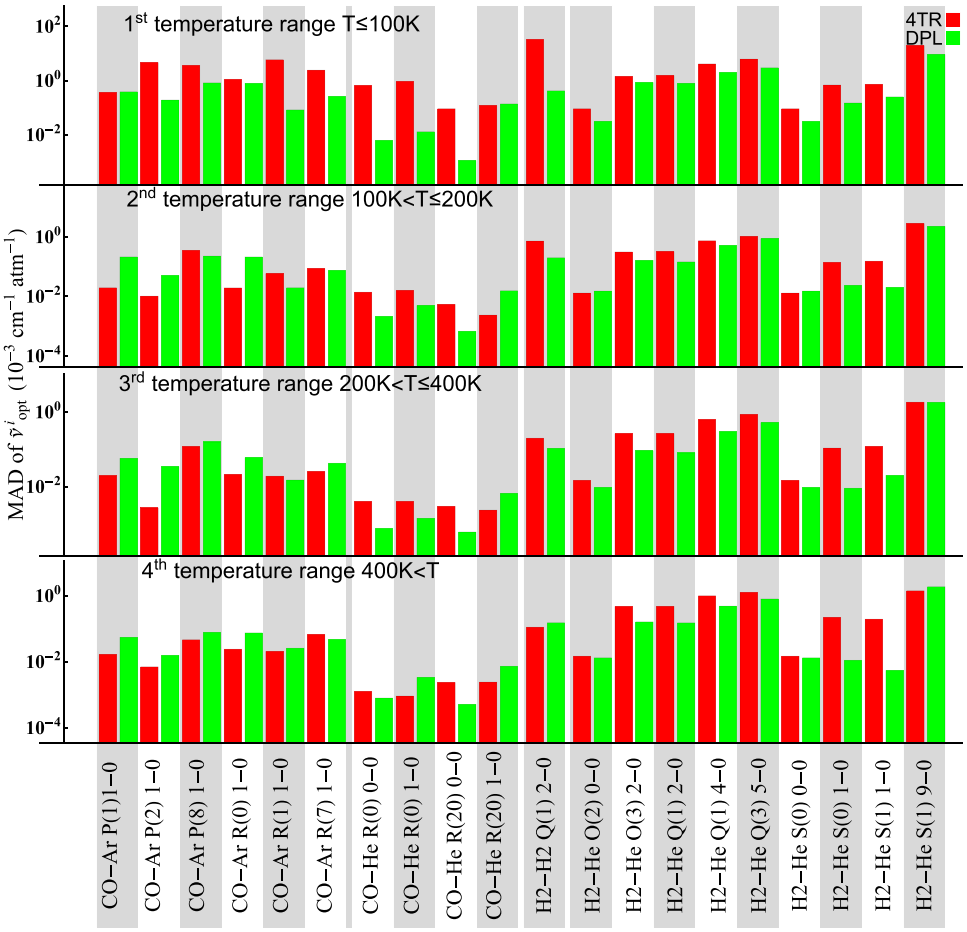

Fig. 12. The MAD for the 4TR and DPL representations of the temperature dependence of the imaginary part of the Dicke parameter, $\tilde{\nu}^{i}_{opt}$ (see text for more details).

resentation that has the same form as for γ_0 and δ_0 discussed in Section 4 (i.e. for each temperature range, single power law and linear functions are taken for real and imaginary parts of the Dicke parameter, respectively):

$$\tilde{\nu}^{r}_{opt}(T) = \tilde{\nu}^{r}_{opt}(T_{ref}) \times \left(\frac{T_{ref}}{T}\right)^{m}, \tag{18}$$

$$\tilde{\nu}^{i}_{opt}(T) = \tilde{\nu}^{i}_{opt}(T_{ref}) + \tilde{\nu}^{i'}_{opt}(T - T_{ref}). \tag{19}$$

Here we take the same reference temperature, T_{ref}, as for the 4TR for γ_0 and δ_0, see Section 4. Moreover, following Section 4, we enforced the continuity of the function on the endpoints of the temperature ranges and performed the same two-step fitting procedure.

The DPL approach has exactly the same form as for the other line-shape parameters discussed in Sections 4 and 5:

$$\tilde{\nu}^{r}_{opt}(T) = r(T_{ref}/T)^{p} + r'(T_{ref}/T)^{p'}, \tag{20}$$

$$\tilde{\nu}^{i}_{opt}(T) = i(T_{ref}/T)^{q} + i'(T_{ref}/T)^{q'}, \tag{21}$$

Also, similar to the other line-shape parameters, here a single DPL function covers all the temperature ranges and $T_{ref} = 296$ K.

6.2. Results and comparison

In Figs. 9 and 10, we show the full temperature dependences of the $\tilde{\nu}^{r}_{opt}$ and $\tilde{\nu}^{i}_{opt}$ parameters determined from our quantum scattering calculations and a comparison of their 4TR and DPL approximations for the same four lines as in Figs. 5 and 6. In Figs. 11 and 12, we compare the MAD for 4TR and DPL for all the cases considered here.

The temperature dependence of the real part of the Dicke parameter, $\tilde{\nu}^{r}_{opt}$, usually decays monotonically with the temperature and can easily be described by a single power-law function, see Fig. 9. For molecular hydrogen, it directly follows from the fact that, in this case, the $\tilde{\nu}^{r}_{opt}$ parameter is close to the frequency of the velocity-changing collisions (that is calculated from the diffusion coefficient). In most of the cases considered here, the 4TR reproduces the *ab inito* temperature dependences more accurately than the DPL, especially in the prioritized, 2nd and 3rd temperature ranges where 4TR reaches sub-percent accuracy for almost all the considered transitions, see Fig. 11. Despite its higher accuracy, it needs to be noted that 4TR requires 8 parameters to represent the full temperature dependence of the $\tilde{\nu}^{r}_{opt}$ parameter, while the DPL representation requires only 4 parameters.

The behavior of the temperature dependence of the imaginary part of the Dicke parameter, $\tilde{\nu}^{i}_{opt}$, depends on the molecular system, see Figs. 10 and 12. In the cases when the temperature dependence is monotonic, both methods provide a good approximation but, usually, DPL is slightly more accurate, see the two bottom panels in Fig. 10. However, if the function exhibits at least one extremum, see the two upper panels in Fig. 10, the 4TR approach shows more flexibility than DPL due to the larger number of the fitted parameters. In Figure 12, we compare the performance of the DPL and 4TR for $\tilde{\nu}^{i}_{opt}$ for all the considered lines.

Table 1
HITRAN parametrization of the DPL temperature dependence of the beyond-Voigt line-shape parameters. In case of the Voigt profile only the first two parameters, γ_0(T) and δ_0(T), should be considered.

Description of the parameters	The symbols of the line-shape parameter [cm^{-1}/atm]	DPL parametrization of the temperature dependence of the line-shape parameters				The formulas illustrating how the parameters should be translated into the line-shape parameters (T_{ref} = 296 K).
		Coefficient 1	Coefficient 2	Exponent 1	Exponent 2	
Pressure broadening	γ_0(T)	g_0	g'_0	n	n′	$\gamma_0(T) = g_0(T_{ref}/T)^{n}+g'_0(T_{ref}/T)^{n'}$
Pressure shift	δ_0(T)	d_0	d'_0	m	m′	$\delta_0(T) = d_0(T_{ref}/T)^{m}+d'_0(T_{ref}/T)^{m'}$
Speed dependence of the pressure broadening	γ_2(T)	g_2	g'_2	j	j′	$\gamma_2(T) = g_2(T_{ref}/T)^{j}+g'_2(T_{ref}/T)^{j'}$
Speed dependence of the pressure shift	δ_2(T)	d_2	d'_2	k	k′	$\delta_2(T) = d_2(T_{ref}/T)^{k}+d'_2(T_{ref}/T)^{k'}$
Real part of the Dicke parameter	$\tilde{\nu}^{r}_{opt}$(T)	r	r′	p	p′	$\tilde{\nu}^{r}_{opt}(T) = r(T_{ref}/T)^{p}+r'(T_{ref}/T)^{p'}$
Imaginary part of the Dicke parameter	$\tilde{\nu}^{i}_{opt}$(T)	i	i′	q	q′	$\tilde{\nu}^{i}_{opt}(T) = i(T_{ref}/T)^{q}+i'(T_{ref}/T)^{q'}$

7. The DPL representation for the HITRAN database

The full set of the coefficients that is needed to represent the DPL temperature dependencies of all the six line-shape parameters (i.e.: γ_0, δ_0, γ_2, δ_2, $\tilde{\nu}^{r}_{opt}$ and $\tilde{\nu}^{r}_{opt}$) described in Sections 4 - 6 consists of 24 coefficients per one molecular transition (4 coefficients per each line-shape parameter), see Table 1. The structure of this parametrization is simpler and requires three parameters fewer than the 4TR parametrization adopted in HITRAN2016 [1,3] (cf. Tab. 7 in Ref. [3]).

8. Conclusion

In this article, we analyzed the problem of seeking an optimal simple analytical representation of temperature dependences of collisional line-shape parameters that can be adopted in the HITRAN database. We used our *ab initio* fully quantum and semiclassical collisional line-shape calculations to compare the 4TR representation, adopted in the HITRAN database in 2016 [1], with the DPL representation. We considered two basic collisional line-shape parameters (γ_0 and δ_0) that enter into the Voigt profile and four beyond-Voigt line-shape parameters (γ_2, δ_2, $\tilde{\nu}^{r}_{opt}$, $\tilde{\nu}^{i}_{opt}$). We demonstrated that DPL gives better overall approximation of the temperature dependences than 4TR. It should be emphasized that DPL requires fewer parameters and its structure is much simpler and more self-consistent than the structure of 4TR. The DPL datasets can be easily implemented into the HITRAN relational database structure due to its flexibility [57]. We present a DPL parametrization for Voigt and beyond-Voigt line profiles that will be adopted in the HITRAN database.

We also discussed the problem of the Hartmann-Tran profile parametrization in which the correlation parameter, η, and frequency of the velocity-changing collisions parameter, ν_{vc}, diverge to infinity when the collisional shift crosses zero. We demonstrate that this issue can be resolved by using a direct parametrization with a complex Dicke parameter, ν_{opt}, instead of η and ν_{vc} that were adopted in the HT profile.

One should be aware that when modeling spectra of hot environments, the usage of the HITEMP [2] database rather than HITRAN is strongly advised. The HITRAN database targets a range of temperatures that does not substantially exceed those encountered on the Earth and with an exception of a few diatomic molecules (NO, OH, HF, HCl, HBr, HI and H_2) does not provide enough transitions. It is worth mentioning that if the temperature range covered in the experiments is not extensive it is better to fix the parameters associated with the second exponent term to be 0 and effectively use a single power law. We also recommend that in the case when there is a sufficient extent of data to fit to the DPL, one should report the new data in both new DPL and traditional single-power law formats if possible. This will allow researchers that work with the room temperature environment to continue using existing radiative transfer codes.

Acknowledgments

We thank Jean-Michel Hartmann and Ha Tran for the discussion and their remarks regarding the parameterization of the Hartmann-Tran profile and the strategy for improving accuracy when the parameters of the Hartmann-Tran profile are based on *ab initio* calculations. NS, HJ and PW contribution is supported by the National Science Centre in Poland through projects nos. 2015/19/D/ST2/02195 and 2018/31/B/ST2/00720. HC acknowledges the support by the National Science Centre in Poland through project no. 2014/15/B/ST4/04551. GK acknowledges the support by the National Science Centre, Poland through project nos. 2016/21/N/ST2/00334 and 2017/24/T/ST2/00242. RRG and BV are pleased to acknowledge support of this research by the National Science Foundation through grant no. AGS-1622676. Any opinions, findings, and conclusions or recommendations expressed in this material are those of the authors and do not necessarily reflect the views of the National Science Foundation. The project is co-financed by the Polish National Agency for Academic Exchange under the PHC Polonium program (dec. PPN/X/PS/318/2018). The HITRAN database is supported by NASA AURA NNX17AI78G and NASA PDART NNX16AG51G grants.

Appendix A. Temperature dependences of the HT profile $\tilde{\nu}_{vc}$ and η parameters

In this section, we compare the parametrization of the velocity-changing collisions employed in this paper and those used in the HT profile. Following the convention adopted in this paper, the total collisional operator, $\hat{S}$, that enters the line-shape theory can be written as

$$\hat{S}/p = -(\gamma_0 + i\delta_0) - (\gamma_2 + i\delta_2)b(v) + (\tilde{\nu}^{r}_{opt} + i\tilde{\nu}^{i}_{opt})\hat{M}, \quad (A.1)$$

where $\tilde{\nu}_{opt}$ is the speed-averaged Dicke parameter, see Eq. (4) (here we neglect the speed dependence of $\tilde{\nu}_{opt}$, see Appendix B). $b(v) = (v^2/v_m^2 - 3/2)$, v_m is the most probable speed of an active molecule, p is pressure and $\hat{M}$ is a normalized velocity-changing operator. Depending on the choice of the line-shape profile, $\hat{M}$ can

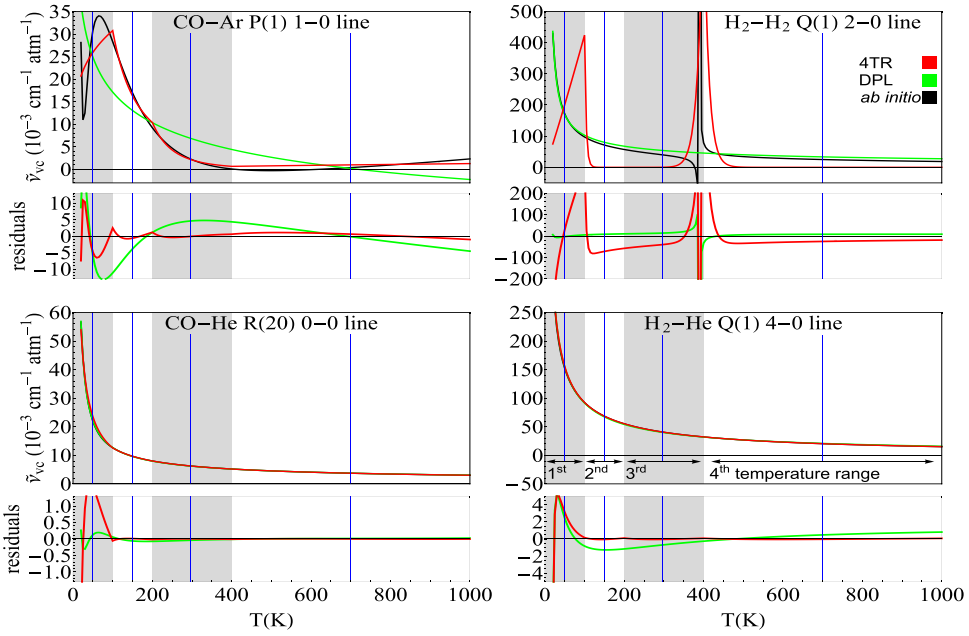

Fig. A1. Temperature dependences of the HT profile frequency of the velocity-changing collisions, $\tilde{\nu}_{vc}$, [16,33,34] determined from the *ab initio* $\tilde{\nu}_{opt}$, γ_0 and δ_0 parameters, see Eqs. 14 and 15, (black lines) and its 4TR and DPL approximations (red and green lines, respectively). To resolve overlapped curves below every graph we show the absolute residuals (the same color notation). The residuals are in the same units as the main plots, i.e., 10^{-3}cm^{-1}atm^{-1}.

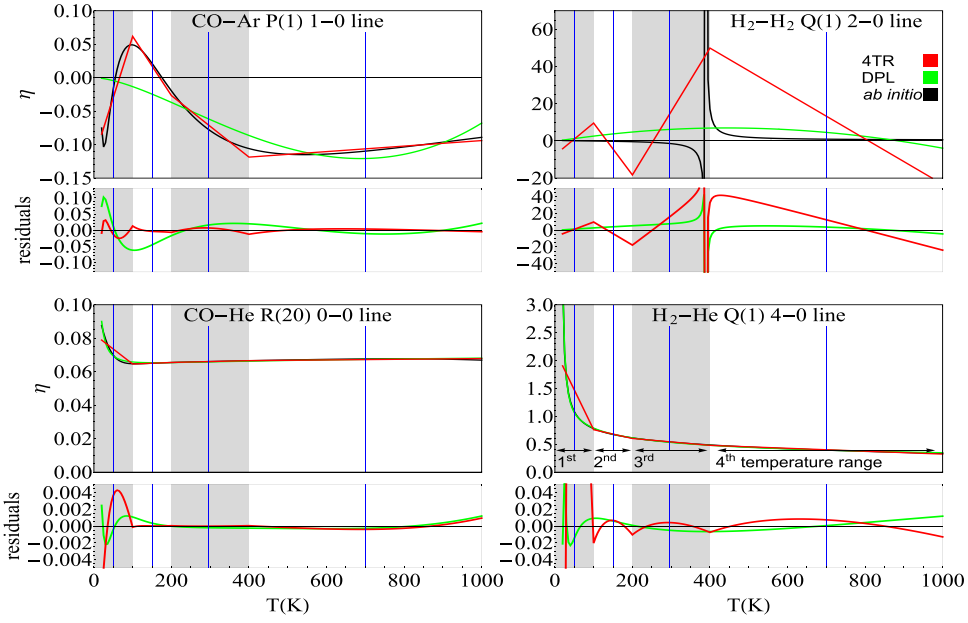

Fig. A2. Temperature dependences of the HT profile correlation parameter, η, [16,33,34] determined from the *ab initio* $\tilde{\nu}_{opt}$ and δ_0 parameters, see Eq. 15, (black lines) and its 4TR and DPL approximations (red and green lines, respectively). To resolve overlapped curves below every graph we show the absolute residuals (the same color notation). The residuals are in the same units as the main plots, i.e., 10^{-3}cm^{-1}atm^{-1}.

be modeled with simple hard-collision [58] (used in the HT profile) or soft-collision [59] operators, or by one of more sophisticated operators like Keilson-Storer [60], billiard-ball [30,31] or Blackmore [32,61], just to mention a few.

Within the convention adopted in the HT profile, the total collisional operator, $\hat{S}_{HTp}$, can be written as

$$\hat{S}_{HTp}/p = -(\gamma_0 + i\delta_0) - (\gamma_2 + i\delta_2)b(v) + (\tilde{\nu}_{vc} - \eta(\gamma_0 + i\delta_0))\hat{M}. \tag{A.2}$$

To make a direct comparison of the velocity-changing parts in Eqs. (A.1) and (A.2), we neglect the speed dependence of the $\tilde{\nu}_{opt} = \tilde{\nu}_{vc} - \eta(\gamma_0 + i\delta_0)$ term in Eq. (A.2). Although this speed dependence is present in the HT profile, we show that it is not consistent with the speed dependence determined directly from quantum-scattering calculations, see Appendix B for details. In Figs. A1 and A2, we show the temperature dependences of $\tilde{\nu}_{vc}(T)$ and $\eta(T)$ and their DPL and 4TR approximations (as deduced from Eqs. (16) and (17). It should be noted that in HITRAN2016 [1,3] the temperature dependence of $\tilde{\nu}_{vc}$ was represented by a single power-law function and η was temperature independent; both of them perform clearly much worse than DPL, therefore in Figs. A1 and A2 we compare DPL with 4TR having the same form as for γ_0 and δ_0, see Section 4.

In the comparison of Eqs. (A.1) and (A.2), i.e. $\tilde{\nu}_{opt}$ representation studied in this paper and that adopted in the HT profile, four main features can be recognized:

- A major practical difficulty related to the convention from Eq. (A.2) is that the $\tilde{\nu}_{vc}(T)$ and $\eta(T)$ functions diverges to $\pm\infty$ when $\delta_0(T)$ crosses zero, see Fig. 2. We show an example of such behavior in the upper right panels in Figs. A1 and A2.
- For most molecular lines, the complex Dicke parameter, $\tilde{\nu}_{opt}$, is dominated by its real part (i.e. $\tilde{\nu}^{r}_{opt} \gg \tilde{\nu}^{i}_{opt}$), compare Figs. 9 and 10. The dominating part is well represented by DPL, see Fig. 9. In the HT profile notation the easy-to-represent behavior of $\tilde{\nu}^{i}_{opt}$, for some systems, can be strongly affected by the way in which the $\eta(T)$ parameter is defined. This makes the $\tilde{\nu}_{vc}(T)$ function much more difficult to reproduce with DPL or 4TR than the $\tilde{\nu}^{r}_{opt}(T)$ function, for instance, compare the CO-Ar P(1) 1-0 case in Figs. 9 and A1.
- The explicit decomposition of $\tilde{\nu}_{opt}$ into its real, $\tilde{\nu}^{r}_{opt}$, and imaginary, $\tilde{\nu}^{i}_{opt}$, parts offers a direct access to their lineshape interpretation, i.e., $\tilde{\nu}^{r}_{opt}$ can be associated with the Dicke narrowing (or more sophisticated effects, like a narrowing of collisional inhomogeneous broadening [62]) and $\tilde{\nu}^{i}_{opt}$ with line asymmetry. In the HT profile parameterization, the $\tilde{\nu}_{vc}$ and η parameters are expressed not only in terms of real and imaginary parts of $\tilde{\nu}_{opt}$, but also in terms of the γ_0 and δ_0 parameters, which makes their interpretation much less straightforward.
- Within the HT profile approach, the complex Dicke parameter is expressed as $\tilde{\nu}_{opt} = \tilde{\nu}_{vc} - \eta(\gamma_0 + i\delta_0)$. This relation may suggest the following physical interpretation: $\tilde{\nu}_{vc}$ is the frequency of the velocity-changing collisions determined from the diffusion coefficient and η is a correlation parameter defining a fraction of molecules (which undergo velocity-changing collisions) being damped or dephased (within this interpretation the rates of the damping and dephasing would be given by γ_0 and δ_0). Here we show that such a picture may be misleading. The $\tilde{\nu}_{opt}$ parameter, calculated from the Generalized Hess Model (GHM) [63], can be written as $\tilde{\nu}_{opt} = (2/3)M_2\omega_1^{11} - M_2(\gamma_0 + i\delta_0)$ [29], where ω_1^{11} is a collision integral of a proper generalized spectroscopic cross section [22,24]. When this generalized spectroscopic cross section is replaced with a usual cross section (used for diffusion coefficient determination), then the above formula can be rewritten as $\tilde{\nu}_{opt} = \tilde{\nu}_{vc} - M_2(\gamma_0 + i\delta_0)$. This shows that the η parameter is simply equal to the mass ratio, M_2. The information about the difference between optical and usual velocity-changing collisions rates is stored in the $(2/3)M_2\omega_1^{11}$ term (which is a complex number) rather than in η, see also the discussion in Appendix B in Ref. [29].

As a result of the above considerations, in this paper we recommend to use in the HITRAN database the straightforward representation of the complex Dicke parameter, i.e., $\tilde{\nu}_{opt} = \tilde{\nu}^{r}_{opt} + i\tilde{\nu}^{i}_{opt}$ for both the hard- and soft-collision models.

Appendix B. Speed dependence of the $\tilde{\nu}_{opt}$ parameter

In this Appendix, we compare the speed dependence of the Dicke parameter obtained from our *ab initio* quantum scattering calculations, see Appendix C, with the one adopted in the HT profile [16,33,34], see also the analysis in Ref. [64]. Within the HT model [16,33,34], the speed-dependent Dicke parameter is defined as $\tilde{\nu}_{opt}(v) = \tilde{\nu}_{vc} - \eta(\gamma(v) + i\delta(v))$. Taking the quadratic expressions for $\gamma(v)$ and $\delta(v)$, the HT profile speed dependence of the real and imaginary parts of the Dicke parameter can be written as

$$\tilde{\nu}^{r}_{opt}(v) = \tilde{\nu}_{vc} - \eta\left(\gamma_0 + \gamma_2\left(\frac{v^2}{v_m^2} - \frac{3}{2}\right)\right), \tag{B.1}$$

$$\tilde{\nu}^{i}_{opt}(v) = -\eta\left(\delta_0 + \delta_2\left(\frac{v^2}{v_m^2} - \frac{3}{2}\right)\right). \tag{B.2}$$

The results of the comparison are depicted in Figs. B1 and B2 for the real and imaginary part of the Dicke parameter, respectively.

It should be noted that the interpretation of the speed dependence of $\tilde{\nu}_{opt}$ is not as straightforward as for the case of the γ and δ parameters. The speed dependence of γ and δ simply means that the complex relaxation rate depends on the molecule speed and, as

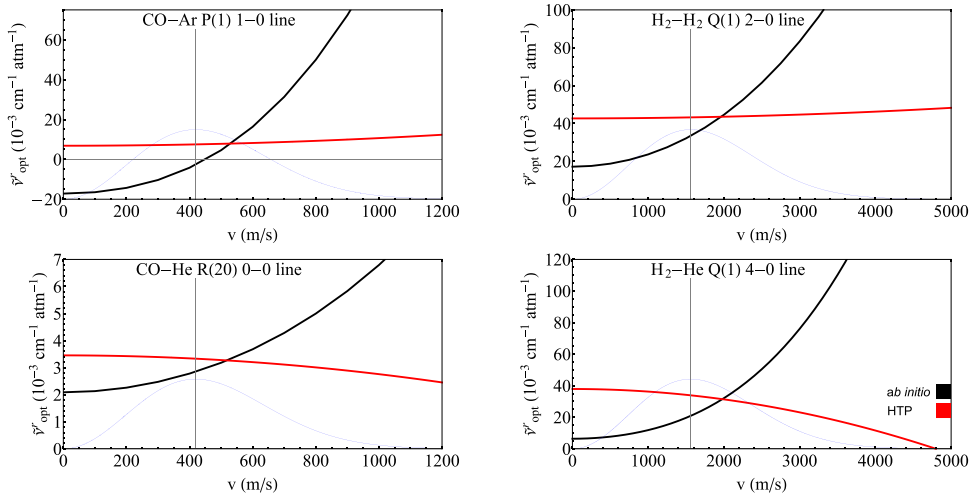

Fig. B1. *Ab initio* speed dependence of the real part of the Dicke parameter, $\tilde{\nu}^{r}_{opt}$, see Eq. C.6b, (black lines) and its approximation adopted in the HT profile, see Eq. (B.1) (red lines). The Maxwell-Boltzmann distributions of the molecular velocities are shown as blue lines and the thin black vertical lines mark the most probable speed. All the data presented here are for $T = 296$ K.

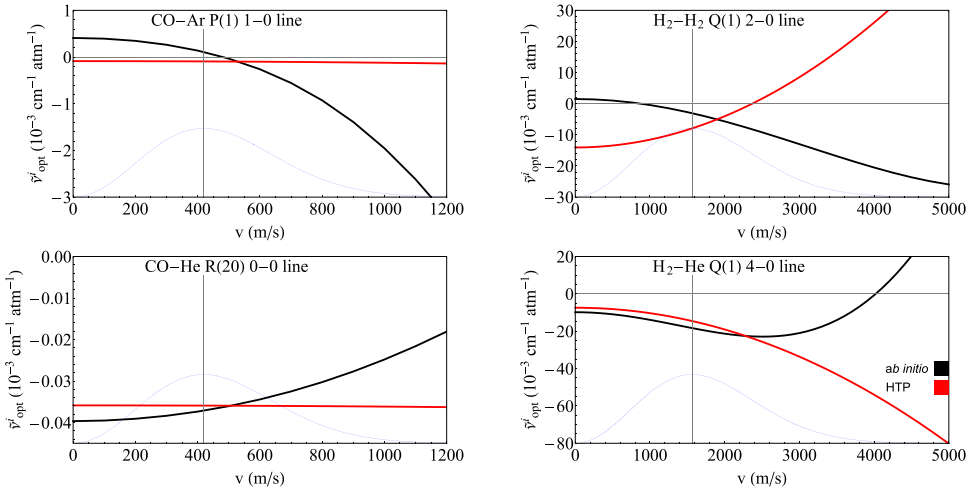

Fig. B2. *Ab initio* speed dependence of the imaginary part of the Dicke parameter, $\widetilde{\nu}^{i}_{\mathrm{opt}}$, see Eq. C.6b, (black lines) and its approximation adopted in the HT profile, see Eq. (B.2) (red lines). The Maxwell-Boltzmann distributions of the molecular velocities are shown as blue lines and the thin black vertical lines mark the most probable speed. All the data presented here are for $T = 296$ K.

it is, directly enters the line-shape model, see Eqs. (A.1) and (A.2). The status of the complex $\widetilde{\nu}_{\mathrm{opt}}$ parameter in the line-shape models is qualitatively different because it does not enter the collisional operator as a scalar function (as it does for $\gamma(v)$ and $\delta(v)$), but it multiplies a velocity-changing operator (see $\hat{M}$ in (A.1) and (A.2)) that already involves some dependence on the active molecule speed, see Fig. 2 in Ref. [65]. For this reason, we assume the $\widetilde{\nu}_{\mathrm{opt}}$ parameter to be speed independent.

Appendix C. Speed dependence of Γ, Δ and ν_{opt} parameters - derivation of the formulas

In this section, we collect the formulas that have been presented in various articles [12,13,24,28,29,66] and rederive the formulas for the speed dependence of the spectroscopic parameters Γ, Δ, and complex ν_{opt}, which are connected to the aforementioned parameters as $\Gamma = p\gamma$, $\Delta = p\delta$, $\nu_{\mathrm{opt}} = p\widetilde{\nu}_{\mathrm{opt}}$. To keep the formulas simple, we assume a structureless perturber. The basic kinetic theory of gases predicts that the collision rate, for a given relative speed v_r, is equal to $nv_r\sigma(v_r)$, where n is the number density of perturber molecules and σ is a usual total cross section. In the same way, one may express a complex relaxation rate of an optical excitation:

$$\Gamma(v_r) + i\Delta(v_r) = \frac{1}{2\pi c} n v_r \sigma_0^q(v_r), \tag{C.1}$$

but σ is replaced with the generalized spectroscopic cross section σ_0^q. The $(2\pi)^{-1}$ factor arises from the fact that, in the actual experiments, the laser frequency is expressed in the unit of frequency and not angular frequency, and c^{-1} comes from the conversion from Hz to cm^{-1}.

Additionally, using a higher-order generalized-spectroscopic cross section, σ_1^q, one may express a complex rate of the optical velocity-changing collisions as (see Appendix A of supplementary materials of Ref. [66])

$$\nu_{\mathrm{opt}}(v_r) = \frac{1}{2\pi c} n v_r M_2 \left(\frac{2}{3} \frac{v_r^2}{v_{\mathrm{rm}}^2} \sigma_1^q(v_r) - \sigma_0^q(v_r) \right), \tag{C.2}$$

where v_{rm} is the most probable relative speed and $M_2 = \frac{m_p}{m+m_p}$, with m and m_p being the masses of the active and perturbing molecules, respectively. On the one hand, direct integration of Eqs. (C.1) and (C.2) over the Maxwellian distribution, $f_m(v_r)$, of relative speeds leads to speed-averaged parameters:

$$\Gamma_0 + i\Delta_0 = \frac{1}{2\pi c} n \int_0^\infty v_r f_m(v_r) \sigma_0^q(v_r) dv_r, \tag{C.3a}$$

$$\nu_{\mathrm{opt}} = \frac{1}{2\pi c} n M_2 \int_0^\infty v_r f_m(v_r) \left(\frac{2}{3} \frac{v_r^2}{v_{\mathrm{rm}}^2} \sigma_1^q(v_r) - \sigma_0^q(v_r) \right) dv_r. \tag{C.3b}$$

On the other hand, one can average the collisional rates over the perturber Maxwellian velocity distribution, $f_{\mathrm{mp}}(\vec{v}_{\mathrm{p}})$, obtaining the speed-dependent spectroscopic parameters (as a function of active molecule speed in the laboratory frame):

$$\Gamma(v) + i\Delta(v) = \int f_{\mathrm{mp}}(\vec{v}_{\mathrm{p}}) (\Gamma(v_r) + i\Delta(v_r)) d^3\vec{v}_p, \tag{C.4a}$$

$$\nu_{\mathrm{opt}}(v) = \int f_{\mathrm{mp}}(\vec{v}_{\mathrm{p}}) (\nu_{\mathrm{opt}}(v_r)) d^3\vec{v}_{\mathrm{p}}. \tag{C.4b}$$

Eqs. (C.4a) and (C.4b) can be expressed explicitly in terms of the generalized spectroscopic cross sections:

$$\Gamma(v) + i\Delta(v) = \frac{1}{2\pi c} n \frac{1}{\pi^{3/2}} \frac{1}{v_{\mathrm{pm}}^3} \int v_r e^{-\frac{(\vec{v}+\vec{v}_r)^2}{v_{\mathrm{pm}}^2}} \sigma_0^q(v_r) d^3\vec{v}_r, \tag{C.5a}$$

$$\nu_{\mathrm{opt}}(v) = \frac{1}{2\pi c} n \frac{1}{\pi^{3/2}} \frac{1}{v_{\mathrm{pm}}^3} M_2 \times \int v_r e^{-\frac{(\vec{v}+\vec{v}_r)^2}{v_{\mathrm{pm}}^2}} \left(\frac{2}{3} \frac{v_r^2}{v_{\mathrm{rm}}^2} \sigma_1^q(v_r) - \sigma_0^q(v_r) \right) d^3\vec{v}_r, \tag{C.5b}$$

where v_{pm} is the most probable perturber speed. After integrating over angular coordinates, one obtains the final expressions (we introduce $x = v_r/v_{\mathrm{pm}}$):

$$\Gamma(v) + i\Delta(v) = \frac{1}{2\pi c} \frac{2nv_{\mathrm{pm}}^2}{\sqrt{\pi} v} e^{-\frac{v^2}{v_{\mathrm{pm}}^2}} \times \int_0^\infty x^2 e^{-x^2} \sigma_0^q(v_r = x v_{\mathrm{pm}}) sinh\left(\frac{2vx}{v_{\mathrm{pm}}} \right) dx, \tag{C.6a}$$

$$\nu_{\mathrm{opt}}(v) = \frac{1}{2\pi c} \frac{2nv_{\mathrm{pm}}^2}{\sqrt{\pi} v} M_2 e^{-\frac{v^2}{v_{\mathrm{pm}}^2}} \times \int_0^\infty x^2 e^{-x^2} \left(\frac{2}{3} M_1 x^2 \sigma_1^q(v_r = x v_{\mathrm{pm}}) - \sigma_0^q(v_r = x v_{\mathrm{pm}}) \right) sinh\left(\frac{2vx}{v_{\mathrm{pm}}} \right) dx, \tag{C.6b}$$

where $M_1 = \frac{m}{m+m_p}$.

References

[1] Gordon IE, Rothman LS, Hill C, Kochanov RV, Tan Y, Bernath PF, et al. The HITRAN2016 molecular spectroscopic database. J Quant Spectrosc Radiat Transfer 2017;203:3–69. doi:10.1016/j.jqsrt.2017.06.038.

[2] Rothman LS, Gordon IE, Barber RJ, Dothe H, Gamache RR, Goldman A, et al. HITEMP, the high-temperature molecular spectroscopic database. J Quant Spectrosc Radiat Transfer 2010;111:2139–50. doi:10.1016/j.jqsrt.2010.05.001.

[3] Wcisło P, Gordon IE, Tran H, Tan Y, Hu SM, Campargue A, et al. The implementation of non-Voigt line profiles in the HITRAN database: H_2 case study. J Quant Spectrosc Radiat Transfer 2016;177:75–91. doi:10.1016/j.jqsrt.2016.01.024.

[4] Gamache RR, Vispoel B. On the temperature dependence of half-widths and line shifts for molecular transitions in the microwave and infrared regions. J Quant Spectrosc Radiat Transfer 2018;217:440–52. doi:10.1016/j.jqsrt.2018.05.019.

[5] Almodovar C, Spearrin R, Hanson RK. Two-color laser absorption near 5 μm for temperature and nitric oxide sensing in high-temperature gases. J Quant Spectrosc Radiat Transfer 2017;203:572–81. doi:10.1016/j.jqsrt.2017.03.003.

[6] Sur R, Peng WY, Strand C, Spearrin R, Jeffries JB, Hanson RK, et al. Mid-infrared laser absorption spectroscopy of NO_2 at elevated temperatures. J Quant Spectrosc Radiat Transfer 2016;187:364–74. doi:10.1016/j.jqsrt.2016.10.016.

[7] Schroeder PJ, Cich MJ, Yang J, Giorgetta FR, Swann WC, Coddington I, et al. Speed-dependent Voigt lineshape parameter database from dual frequency comb measurements up to 1305K. part I: Pure H_2O absorption, 6801-7188 cm^{-1}. J Quant Spectrosc Radiat Transfer 2018;210:240–50. doi:10.1016/j.jqsrt.2018.02.025.

[8] Cybulski H, Bielski A, Ciuryło R, Szudy J, Trawiski RS. Power-law temperature dependence of collision broadening and shift of atomic and molecular rovibronic lines. J Quant Spectrosc Radiat Transfer 2013;120:90–103. doi:10.1016/j.jqsrt.2013.02.020.

[9] Lee J-M, Fletcher L, Irwin P. Optimal estimation retrievals of the atmospheric structure and composition of HD 189733b from secondary eclipse spectroscopy. Mon Notices Royal Astron Soc 2011;420:170–82. doi:10.1111/j.1365-2966.2011.20013.x.

[10] Angelo I, Hu R. A case for an atmosphere on Super–Earth 55 Cancri e. Astron J 2017;154:6. doi:10.3847/1538-3881/aa9278.

[11] Berman PR. Speed–dependent collisional width and shift parameters in spectral profiles. J Quant Spectrosc Radiat Transfer 1972;12:1331–42. doi:10.1016/0022-4073(72)90189-6.

[12] Ward J, Cooper J, Smith EW. Correlation effects in the theory of combined doppler and pressure broadening I. Classical theory. J Quant Spectrosc Radiat Transfer 1974;14:555–90. doi:10.1016/0022-4073(74)90036-3.

[13] Pickett HM. Effects of velocity averaging on the shapes of absorption lines. J Chem Phys 1980;73:6090–4. doi:10.1063/1.440145.

[14] Lance B, Blanquet G, Walrand J, Populaire J-C, Bouanich J-P, Robert D. Inhomogeneous lineshape profiles of C_2H_2 perturbed by Xe. J Mol Spectrosc 1999;197:32–45. doi:10.1006/jmsp.1999.7892.

[15] Hartmann J-M, Boulet C, Robert D. Collisional Effects on Molecular Spectra. Laboratory Experiments and Models, Consequences for Applications. Amsterdam: Elsevier Science; 2008.

[16] Tran H, Ngo NH, Hartmann J-M. Efficient computation of some speed-dependent isolated line profiles. J Quant Spectrosc Radiat Transfer 2013;129:199–203. doi:10.1016/j.jqsrt.2013.06.015.

[17] Green S. Rotational excitation in H_2-H_2 collisions: Close-coupling calculations. J Chem Phys 1975;62:2271. doi:10.1063/1.430752.

[18] Thibault F, Wcisło P, Ciuryło R. A test of H_2-He potential energy surfaces. Eur Phys J D 2014;70:236. doi:10.1140/epjd/e2016-70114-9.

[19] Hutson JM, Green S. Molscat version14, Collaborative Computational Project 6 of the UK Science and Engineering Research Council, Daresbury Laboratory, UK, 1995.

[20] Ben-Reuven A. Symmetry considerations in pressure-broadening theory. Phys Rev 1966;141:34. doi:10.1103/PhysRev.141.34.

[21] Ben-Reuven A. Impact broadening of microwave spectra. Phys Rev 1966;145:7. doi:10.1103/PhysRev.145.7.

[22] Monchick L, Hunter L. Diatomic-diatomic molecular collision integrals for pressure broadening and Dicke narrowing: a generalization of Hess's theory. J Chem Phys 1986;85:713. doi:10.1063/1.451277.

[23] Schaefer J, Monchick L. Line broadening of HD immersed in He and H_2 gas. Astron Astrophys 1992;859:265.

[24] Corey GC, McCourt FR. Dicke narrowing and collisional broadening of spectral lines in dilute molecular gases. J Chem Phys 1984;81:2318–29. doi:10.1063/1.447930.

[25] Ciuryło R, Jaworski R, Jurkowski J, Pine AS, Szudy J. Spectral line shapes modeled by a quadratic speed-dependent Galatry profile. Phys Rev A 2001;63:032507. doi:10.1103/PhysRevA.63.032507.

[26] Priem D, Rohart F, Colmont J-M, Wlodarczak G, Bouanich J-P. Lineshape study of the J=3 ← 2 rotational transition of CO perturbed by N_2 and O_2. J Mol Struct 2000;517–518:435–54. doi:10.1016/S0022-2860(99)00268-9.

[27] Rohart F, Mader H, Nicolaisen H. Speed dependence of rotational relaxation induced by foreign gas collisions: Studies on CH_3F by millimeter wave coherent transients. J Chem Phys 1994;101:6475–86. doi:10.1063/1.468342.

[28] Wcisło P, Thibault F, Zaborowski M, Wójtewicz S, Cygan A, Kowzan G, et al. Accurate deuterium spectroscopy for fundamental studies. J Quant Spectrosc Radiat Transfer 2018;213:41. doi:10.1016/j.jqsrt.2018.04.011.

[29] Thibault F, Patkowski K, Żuchowski P, Jóźwiak H, Wcisło P, Ciuryło R. Rovibrational line-shape parameters for H_2 in He and new H_2-He potential energy surface. J Quant Spectrosc Radiat Transfer 2017;202:308. doi:10.1016/j.jqsrt.2017.08.014.

[30] Lindenfeld MJ. Self–structure factor of hardsphere gases for arbitrary ratio of bath to test particle masses. J Chem Phys 1980;73:5817–29. doi:10.1063/1.440066.

[31] Liao PF, Bjorkholm JE, Berman PR. Effects of velocity-changing collisions on two-photon and stepwise-absorption spectroscopic line shapes. Phys Rev A 1980;21:1927–38. doi:10.1103/PhysRevA.21.1927.

[32] Blackmore R. A modified Boltzmann kinetic equation for line shape functions. J Chem Phys 1987;87:791–800.

[33] Tran H, Ngo NH, Hartmann J-M. Erratum to coefficient computation of some speed-dependent isolated line profiles[J. Quant. Spectrosc. Radiat. Transfer 2013; 129: 199–203]. J Quant Spectrosc Radiat Transfer 2014;134:104. doi:10.1016/j.jqsrt.2013.10.015.

[34] Tennyson J, Bernath PF, Campargue A, Csszr AG, Daumont L, Gamache RR, et al. Recommended isolated-line profile for representing high-resolution spectroscopic transitions (IUPAC technical report). Pure Appl Chem 2014;86:1931–43. doi:10.1515/pac-2014-0208.

[35] Konefał M, Słowiński M, Zaborowski M, Ciuryło R, Lisak D, Wcisło P. Submitted to J. Quant. Spectrosc. Radiat. Transfer.

[36] Private communication with J.-M. Hartmann (2018).

[37] Wcisło P, Lisak D, Ciuryło R, Pine AS. Multispectrum-fitting of phenomenological collisional line-shape models to a speed-dependent Blackmore profile for spectroscopic analysis and databases. J Phys: Conf Series 2017;810:012061. doi:10.1088/1742-6596/810/1/012061.

[38] Ngo N, Hartmann J-M. A strategy to complete databases with parameters of refined line shapes and its test for CO in He, Ar and Kr. J Quant Spectrosc Radiat Transfer 2017;203:334–40. doi:10.1016/j.jqsrt.2017.01.031.

[39] Bakr BW, Smith DGA, Patkowski K. Highly accurate potential energy surface for the He-H_2 dimer. J Chem Phys 2013;139:144305. doi:10.1063/1.4824299.

[40] Jóźwiak H, Thibault F, Stolarczyk N, Wcisło P. Ab initio line-shape calculations for the S and O branches of H_2 perturbed by He. J Quant Spectrosc Radiat Transfer 2018;219:313. doi:10.1016/j.jqsrt.2018.08.023.

[41] Alexander M, Manolopoulos D. A stable linear reference potential algorithm for solution of the quantum close–coupled equations in molecular scattering theory. J Chem Phys 1987;86:2044. doi:10.1063/1.452154.

[42] Garberoglio G, Jankowski P, Szalewicz K, Harvey AH. Second virial coefficients of H_2 and its isotopologues from a six-dimensional potential. J Chem Phys 2012;137:154308. doi:10.1063/1.4757565.

[43] Hinde RJ. A six-dimensional H_2 – H_2 potential energy surface for bound state spectroscopy. J Chem Phys 2008;128:154308. doi:10.1063/1.2826340.

[44] Patkowski K, Cencek W, Jankowski P, Szalewicz K, Mehl JB, Garberoglio G, et al. Potential energy surface for interactions between two hydrogen molecules. J Chem Phys 2008;129:094304. doi:10.1063/1.2975220.

[45] Li G, Gordon IE, Rothman LS, Tan Y, Hu S-M, Kassi S, et al. Rovibrational Line Lists for Nine Isotopologues of the CO Molecule in the $X\ ^1\Sigma^+$ Ground Electronic State. Astrophys J Suppl S 2015;216. doi:10.1088/0067-0049/216/1/15.

[46] Coxon JA, Hajigeorgiou PG. Direct potential fit analysis of the $X\ ^1\Sigma^+$ ground state of CO. J Chem Phys 2004;121:2992–3008. doi:10.1063/1.1768167.

[47] Heijmen TGA, Moszynski R, Wormer PES, van der Avoird A. A new He–CO interaction energy surface with vibrational coordinate dependence. I. Ab initio potential and infrared spectrum. J Chem Phys 1997;107(9921). doi:10.1063/1.475290.

[48] Luo C, Wehr R, Drummond J, May A, Thibault F, Boissoles J, et al. Shifting and broadening in the fundamental band of CO highly diluted in He and Ar: A comparison with theory. J Chem Phys 2001;115:2198–206. doi:10.1063/1.1383049.

[49] Sumiyoshi Y, Endo Y. Three-dimensional potential energy surface of Ar–CO. J Chem Phys 2015;142:024314. doi:10.1063/1.4905268.

[50] Robert D, Bonamy J. Short range force effects in semiclassical molecular line broadening calculation. J Phys France 1979;40. doi:10.1051/jphys:019790040010092300.

[51] Lynch R, Gamache RR, Neshyba SP. Fully complex implementation of the Robert–Bonamy formalism: Half widths and line shifts of H_2O broadened by N_2. J Chem Phys 1996:5711–21. doi:10.1063/1.472416.

[52] Ma Q, Tipping R, Boulet C. Modification of the Robert Bonamy formalism in calculating Lorentzian half-widths and shifts. J Quant Spectrosc Radiat Transfer 2007;103:588–96. doi:10.1016/j.jqsrt.2006.08.001.

[53] Renaud CL, Cleghorn K, Hartmann L, Vispoel B, Gamache RR. Line shape parameters for the H_2O–H_2 collision system for application to exoplanet and planetary atmospheres. Icarus 2018;306:275–84. doi:10.1016/j.icarus.2017.10.016.

[54] Vispoel B, Cavalcanti JH, Gamache RR. Modified complex Robert-Bonamy calculations of line shape parameters and their temperature dependence for water vapor in collision with N_2. J Quant Spectrosc Radiat Transfer 2019;228:79–89. doi:10.1016/j.jqsrt.2019.02.023.

[55] Gamache RR, Laraia AL, Lamouroux J. Half-widths, their temperature dependence, and line shifts for the HDO–CO_2 collision system for applications to CO_2–rich planetary atmospheres. Icarus 2011;213:720–30. doi:10.1016/j.icarus.2011.03.021.

[56] Lamouroux J, Gamache RR, Laraia AL, Hartmann J-M, Boulet C. Semiclassical calculations of half-widths and line shifts for transitions in the 30012 ← 00001 and 30013 ← 00001 bands of CO_2. III: Self collisions. J Quant Spectrosc Radiat Transfer 2012;113:1536–46. doi:10.1016/j.jqsrt.2012.03.035.

[57] Hill C, Gordon IE, Kochanov RV, Barrett L, Wilzewski JS, Rothman LS. HITRAN*online*: An online interface and the flexible representation of spectroscopic data in the HITRAN database. J Quant Spectrosc Radiat Transfer 2016;177:4–14. doi:10.1016/j.jqsrt.2015.12.012.

[58] Bohm D, Gross EP. Theory of plasma oscillations. A. Origin of medium-like behavior. Phys Rev 1949;75:1851–64. doi:10.1103/PhysRev.75.1851.

[59] Chandrasekhar S. Stochastic problems in physics and astronomy. Rev Mod Phys 1943;15:1–89. doi:10.1103/RevModPhys.15.1.

[60] Tran H, Hartmann J-M, Chaussard F, Gupta M. An isolated line-shape model based on the Keilson–Storer function for velocity changes. II. Molecular dynamics simulations and the Q(1) lines for pure H_2. J Chem Phys 2009;131:154303. doi:10.1063/1.3247898.

[61] Wcisło P, Ciuryło R. Influence of the interaction potential shape on the Dicke narrowed spectral line profiles affected by speed-dependent collisional broadening and shifting. J Quant Spectrosc Radiat Transfer 2013;120:36–43. doi:10.1016/j.jqsrt.2013.02.023.

[62] Wcisło P, Thibault F, Cybulski H, Ciuryło R. Strong competition between velocity-changing and phase- or state-changing collisions in H_2 spectra perturbed by Ar. Phys Rev A 2015;91:052505. doi:10.1103/PhysRevA.91.052505.

[63] Hess S. Kinetic theory of spectral line shapes. The transition between doppler broadening and collisional broadening. Physica 1972;61:80–94. doi:10.1016/0031-8914(72)90035-3.

[64] Kowzan G, Wcisło P, Słowiński M, Masłowski P, Viel A, Thibault F. Submitted to J. Quant. Spectrosc. Radiat. Transfer.

[65] Wcisło P, Tran H, Kassi S, Campargue A, Thibault F, Ciuryło R. Velocity-changing collisions in pure H_2 and H_2–Ar mixture. J Chem Phys 2014;141:074301. doi:10.1063/1.4892414.

[66] Martínez RZ, Bermejo D, Thibault F, Wcisło P. Testing the ab initio quantum-scattering calculations for the D_2–He benchmark system with stimulated raman spectroscopy. J of Raman Spectrosc 2018;49:1339–49. doi:10.1002/jrs.5391.